AD-A097 469 MASSACHUSETTS INST OF TECH CAMBRIDGE DEPT OF MATERIA--ETC F/G 11/6
SULFIDE INCLUSIONS IN ELECTROSLAG REMELTED STEELS.(U)
JAN 81 M D BOLDY, T FUJII, D R POIRIER DAAG46-78-C-0032
UNCLASSIFIED AMMRC-TR-81-4 NL

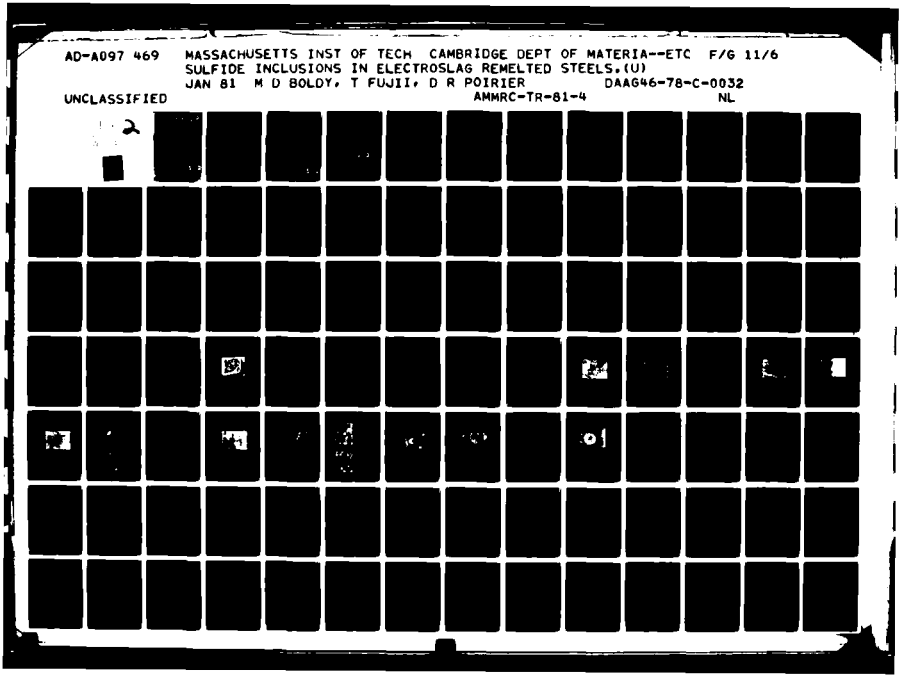

AMMRC TR 81-4

SULFIDE INCLUSIONS IN ELECTROSLAG REMELTED STEELS

January 1981

M. D. Boldy, T. Fujii, D. R. Poirier, and M. C. Flemings

Massachusetts Institute of Technology
Cambridge, Massachusetts 02139

Final Report, Contract Number DAAG46-78-C-0032

Prepared for
ARMY MATERIALS AND MECHANICS RESEARCH CENTER
Watertown, Massachusetts 02172

The findings in this report are not to be construed as an official Department of the Army position, unless so designated by other authorized documents.

Mention of any trade names or manufacturers in this report shall not be construed as advertising nor as an official indorsement or approval of such products or companies by the United States Government.

DISPOSITION INSTRUCTIONS

Destroy this report when it is no longer needed.
Do not return it to the originator.

SULFIDE INCLUSIONS IN ELECTROSLAG REMELTED STEELS

Final Technical Report by

M. D. Boldy, T. Fujii, D. R. Poirier and M. C. Flemings

Massachusetts Institute of Technology

Cambridge, Massachusetts 02139

Final Technical Report

Contract No. DAAG-46-78-C-0032

Approved for public release; distribution unlimited.

Prepared for

ARMY MATERIALS AND MECHANICS RESEARCH CENTER
Watertown, Massachusetts 02172

FOREWORD

This report was prepared by the Casting and Solidification Research Group in the Department of Materials Science and Engineering, Massachusetts Institute of Technology. The report is entitled "Sulfide Inclusions in Electroslag Remelted Steels"; the contract was administered under the technical supervision of G. Bruggeman of the Army Materials and Mechanics Research Center, Watertown, Massachusetts.

TABLE OF CONTENTS

ABSTRACT

The relationships among heat treatment, sulfide inclusion distribution and chemistry were investigated in this work, and the problem of overheating found to be directly related to these parameters.

A basis for comparison was found in microscopic examination of carbon extraction replicas from commercially produced electroslag remelted steel. This showed a direct correlation between sulfide inclusion distribution and overheating. Further investigation characterized a critical cooling rate necessary for overheating to occur.

Methods for eliminating the problem of sulfide inclusions in ESR steels were examined in detail. The simplest is to alter the cooling rate through the overheating range. Either a fast or a very slow cool eliminates the problem. An alternate method of eliminating the problem is to change the chemistry of the steel. These different techniques were examined in this work. All three were tested and proved to be successful in eliminating the sulfide problem.

In an associated study a model to simulate the diffusion controlled coarsening and dissolution kinetics of particles

within a metallic matrix was formulated. Calculations were made and compared with experiments in a model system and on manganese sulfide inclusions in iron. The effect of the manganese and sulfur content was studied. Agreement of the calculations is good.

PART I. SULFIDE INCLUSIONS IN ESR STEEL

I. INTRODUCTION

The problems associated with sulfide inclusions in electroslag remelted steels are identical to those first investigated in air-melted steels after World War II. The problem, normally called "overheating", causes a reduction in the toughness of steel. The fracture surface of an overheated steel has a characteristic faceted appearance. The early investigations determined that overheating is caused by the precipitation of manganese sulfides onto high-temperature austenitic grain boundaries. The precipitation occurs in such a manner that the sulfides form a continuous array of particles throughout the steel. This creates a preferred path for transgranular crack propagation through the room temperature matrix. The characteristic faceted fracture surface is a result of this type of fracture. The separation is occurring at what was a high-temperature austenitic grain boundary.

It was assumed that, with the advent of methods to produce cleaner steels such as electroslag remelting (ESR), the problem would disappear. However, this has not been the case. The use of the secondary refining processes has not eliminated the problem. Despite the fact that these types of processes decrease the sulfur content of the product, the problems

associated with overheating still exist. It has been suggested that the very fine dispersion of sulfides produced throughout the ESR ingot enhances the precipitation problem [17].

The critical step in the thermo-mechanical treatment of a steel seems to be the cooling rate from the overheating range, approximately 1100°C - 1400°C. A critical cooling rate through this austenite region permits the proper precipitation to occur and thus brings on overheating.

The basic problem is to eliminate the problem of sulfide inclusions with a minimum effort. The solutions come in two categories. The first is to change the cooling rate to alter the precipitation kinetics. The other set of solutions involves an alteration in the chemistry of the steel such that manganese sulfides are not stable anywhere in the temperature range encountered in metal processing.

The aim of this research program was to study and characterize the precipitation of manganese sulfides under various conditions that would lead to or possibly eliminate the harmful arrays of inclusions characteristic of overheating. It is important that a direct correlation between the effects of overheating and the microstructural phenomena observed is found. Observations of this type were made on commercially produced

steels rejected for reduced through-the-thickness ductility and on steels with specific chemistry modifications designed to eliminate the problem. The commercially produced steels were assumed to be in the overheated condition.

II. LITERATURE SURVEY

The phenomenon known as overheating was first studied in the years following World War II [1-3]. The initial work was concerned with the identification and definition of the problem. At first, the problem was thought to be a form of another prevalent steelmaking problem of the times known as "burning." It was well known that during the heating cycle for forging and hot working, the use of excessive temperatures produced a severely weakened structure, caused by actual fusion of the grain boundaries. However, even at temperatures below those required for grain boundary fusion, degenerated mechanical properties were not uncommon. Steels in this latter condition became known as "overheated" steels.

The primary work in the late forties [1-3] used several different parameters to indicate the presence of overheating. The appearance of the fracture surface was the first and most important indicator. Figure 1 illustrates the characteristic faceted fracture surface found on overheated steels. The second bit of evidence of overheating was the decrease in impact strength or toughness. In all cases of overheating there is a significant decrease in toughness. The third parameter in use was the overheating temperature, now known as the overheating onset temperature (OOT). This is the

threshold temperature below which there is no evidence of overheating.

Several important discoveries were made as a result of this work. It was found that the OOT was an inherent property of a steel and that it covered a range of temperatures extending upward from 1250°C [2]. More importantly it was determined that the cooling rate from a point within the overheating range was a critical factor. A very rapid or a very slow cooling rate was found to suppress the formation of facets on the fracture surface. The cooling rate necessary for overheating is approximated by air cooling, approximately 50 - 100 °C/min. The final major contribution of this early work was the discovery that the type of steelmaking process used had a significant effect on the overheating characteristics of the steel [3]. It was found that steels made in the electric arc furnaces had lower OOT's than did those steels made in open hearth furnaces. The reason for this phenomenon was not determined until much later.

Later work, reported in the early fifties [4-7], investigated the relationships between cooling rate and overheating in more detail. Preece et al. [4] determined that the critical cooling rate for overheating extended from approximately 10 °C/minute to 1000 °C/minute depending upon

the steel being tested. Figure 2 illustrates a representative set of results. The compositions of the steels used in past experiments are listed in Table 1.

Ko and Hanson [5] were the first researchers to attribute overheating to the precipitation of manganese sulfides onto grain boundaries. Examination of fracture surfaces under a light microscope led them to suggest that as the temperature increased into the overheating range, the number of inclusions on the grain boundaries would increase and thus the severity of overheating. They determined that a slow cooling rate or a long anneal at a temperature below the OOT would decrease the number of inclusions, thus improving the quality of the steel. Other research done at this time [6,7] tended to agree with these findings.

The next series of investigations [10-13] was primarily concerned with the effects of overheating on mechanical properties and with the effects of steel chemistry. Baker and Johnson [11] found that the OOT tended to increase with an increasing sulfur content. They explained this through the hypothesis that fracture via the large elongated sulfides found in the higher sulfur steels would proceed much more easily than fracture along the precipitates formed on the grain boundaries. It seemed reasonable to believe that a higher

TABLE 1: Compositions of Steels Used in Previous Research

Figure Number	Grade	Compositions in Weight Percent									Manufacturing Method
		C	Si	Mn	Ni	Cr	Mo	V	S	Ce	
2	En22	0.37	0.22	0.62	0.23	-	-	-	0.020	-	electric arc
2	En25	0.31	0.24	0.69	0.64	0.56	-	-	0.015	-	electric arc
2	En39	0.12	0.21	0.43	1.11	0.20	-	-	0.020	-	electric arc
4	-	0.32	0.25	0.64	2.56	0.74	0.47	-	0.005	-	electric arc
4	-	0.36	0.26	0.54	3.1	0.79	0.65	0.19	0.005	-	ESR
5	En39B	0.14	0.33	0.33	3.92	1.23	0.25	-	0.007	-	vacuum melt
5	En39B	0.21	0.33	0.24	4.00	1.25	0.25	-	0.006	-	vacuum melt
-	4340	0.38-0.43	0.20-0.35	0.60-0.80	1.65-2.00	0.70-0.90	0.20-0.30	- -	0.040 max	0.011 -	AISI spec.

temperature would be required in order to dissolve the larger amounts of manganese sulfide. Those sulfides that remained in the matrix would tend to grow larger and less harmful. This would explain why a "cleaner" steel would have a lower OOT and thus more of a problem with overheating.

Work done by Ritchie and Knott [12] on chromium-containing manganese-free steels produced some interesting results. Whereas low alloy steels containing manganese required a temperature of 1200°C to 1300°C to induce overheating, the chromium-bearing steels became overheated at temperatures an average of 50°C lower. The responsibility for this decrease in the OOT belongs to the chromium sulfides which dissolve at a lower temperature then the manganese sulfides. They characterized the effect of sulfur content by determining that an increased sulfur content, greater than 0.02 weight percent, would raise the OOT to above 1400°C. The larger sulfides that formed would ease transgranular fracture through these inclusions.

Andrew and Weston [15-18] performed a series of studies on various low sulfur steels. Their first investigation looked at the response of specimen orientation to overheating onset temperature. They found that the OOT was slightly lower in the longitudinal direction than it was in the transverse direction. Later work, on similar steels, characterized the effect of

austenitizing or overheating temperature on the notch toughness of the different orientations. Figure 3 illustrates the findings of this study. As the overheating temperature increases, the equilibrium amount of manganese sulfides that goes into solution will increase. Upon cooling, these sulfides will precipitate onto the grain boundaries and subsequently reduce the toughness and increase the resultant overheating severity.

The other work reported by these researchers [18], looked at overheating in electroslag remelted steels. They were primarily interested in the effects of tempering on the overheated steels. Their findings, presented in Figure 4, show that as the tempering temperature increases, the notch toughness will also increase. This is due in part to the ripening of the sulfides. As the sulfides grow fewer in number and larger in size, fracture along what was an austenitic grain boundary becomes energetically less feasible. Another interesting finding of this study was that an ESR steel consistently had a lower toughness than the electric arc steel heat treated at the same temperature, even with equivalent sulfur contents. This can be explained by the finer and more uniform dispersion of manganese sulfides found in the ESR steels.

More recent work [14,19] has focused on the effect of chemistry alterations on the overheating characteristics of steels. Nutting [19] has found that an alteration in the manganese content of the steel can have a positive effect on the steel. Figure 6 illustrates the results he obtained. A reduction in the manganese content will increase the sulfur solubility in the austenite along with the obvious removal of the manganese to tie up the sulfur. Increasing the manganese content lowers the sulfur solubility, thus preventing the sulfides from going into solution and subsequently precipitating out. However, it is possible to enhance temper embrittlement by this method.

Glue, et al [14], have found that an addition of cerium, even in the presence of manganese, will produce a change in the sulfide type. An addition of cerium, in a Ce/S ratio of 2:1 can completely eliminate the characteristic overheating fracture. The sulfur will combine with the cerium to produce higher melting point complex sulfides and oxysulfides. Figure 6 illustrates the effect of the cerium addition on the impact strength of a treated steel. It is obvious that the use of a rare-earth addition can be used to at least alleviate the problem of overheating.

III. EXPERIMENTAL PROCEDURE

A. Materials

All of the experiments utilized steels of nominal AISI 4340 composition prepared by electroslag remelting. This steel was chosen because of its widespread use in industrial applications. It is also a common steel used in electroslag remelting. The first three lots of steel were commercially produced while the steels with altered compositions were produced for this research program. Except for the steel with rare earth additions, these lots were furnished by the Army Mechanics and Materials Research Center at Watertown, Massachusetts (AMMRC). The steel with the rare-earth additions was produced by the United States Steel Research Center. The last lot was produced by vacuum induction melting rather than ESR. The compositions for all of these lots are listed in Table 2.

B. Procedure

The basic aim of this project was to examine the inclusion structure of steels after various heat treating steps and to compare those structures with those found in overheated steels. Since overheating is the problem at hand, the temperature range selected for the heat treatments approximated the overheating range, 1100°C - 1400°C. These temperatures also lie in the range of industrial forging temperatures.

TABLE 2: Compositions of Experimentsl 4340 Steels

	Compositions in Weight Percent								
Code	C	Si	Mn	Ni	Cr	Mo	Al	S	Comments
C7T	0.43	0.35	0.72	1.83	0.90	0.31	-	0.007	
A3	0.40	0.22	0.77	1.78	0.80	0.24	-	0.003	
L3	0.36	0.26	0.74	1.80	0.77	0.26	-	0.001	
69	0.42	0.01	0.06	1.80	0.86	0.26	0.02	0.005	
71	0.32	1.57	0.84	1.78	0.82	0.25	1.41	0.002	
76	0.43	0.40	3.58	1.82	0.84	0.27	0.042	0.003	
RE	0.37	0.27	0.70	1.81	0.78	0.25	0.028	0.010	Ce-0.12, La 0.012
4340	0.38-0.43	0.20-0.35	0.60-0.80	1.65-2.00	0.70-0.90	0.20-0.30	-	0.040 max	AISI spec.

Temperatures selected were: 1100°C, 1250°C and 1375°C. The samples were cut from the pieces supplied by AMMRC and encapsulated in quartz tubing under an argon atmosphere. This was done to prevent atmospheric contaimination at the temperatures used. The specimens were held at temperature for approximately one hour to insure that equilibrium would be attained. The samples were then cooled at three different rates. Specimens from each temperature used were oil quenched, air cooled or furnace cooled. The specimens containing the rare-earth elements were treated somewhat differently. All of these samples were air-cooled through the overheating range. The specimens were heat treated at 50°C intervals in the temperature range of 1100°C - 1400°C. The furnace cooling rate was found to be in the range from 5 °C/minute to 10 °C/minute. The air cooling rate was approximately 50 °C/minute to 100 °C/minute. The oil quench reached a cooling rate of approximately 200 °C/minute to 300 °C/minute. This enabled the researchers to correlate the inclusion structure with the cooling rate, the critical step in overheating. To insure the uniformity of the matrix material for all of the samples, they were all heat treated at 800°C for one-half hour and subsequently oil quenched. This produced a uniform martensitic matrix without altering the sulfide distribution. Work performed by Fujii [30] has shown that the kinetics of

sulfide dissolution are slow enough to prevent any changes with this time and temperature.

C. Metallography

Each specimen, after heat treatment, was mounted in Bakelite. Where applicable, the short transverse direction was investigated. Each sample was polished and etched using a weak nital solution. The samples were then subjected to a carbon extraction replication procedure for subsequent examination in an electron microscope. This procedure produces a replica of carbon with the inclusions from the original surface imbedded in the carbon film. The procedure is described in the appendix.

Each sample was examined to determine the relative inclusion size, number and distribution with an emphasis on the distribution. In general, the small number and size of the particles precluded any attempt at obtaining a quantitative measure of the inclusion number density. However, it is possible to qualitatively characterize the samples with respect to one another. The inclusions were identified with the use of the x-ray analysis capability incorporated into the electron microscope system.

IV. RESULTS

A. Commercially Produced Steels

1. As-Received material

These experiments focused on the commercially produced 4340 steels. Three lots of material, designated as C7T, A3 and L3 were used in this work. All of these steels were produced using the electroslag remelting technique. The compositions for these steels are listed in Table 2.

The initial observations on the as-received samples were made to form a basis of comparison for the later work. The three lots of steel had been produced for the same application by different suppliers. The lot designated as L3 was rejected, because of decreased ductility, assumed to be caused by overheating. The other lots, A3 and C7T, were found to be marginally acceptable and completely acceptable respectively.

Upon microscopic examination, the steel designated as acceptable exhibited no characteristic or unusual inclusion distribution. An examination of Figure 7, a typical site in the material, reveals that very few inclusions exist in the material. This has been taken as representative of a superior steel.

The poor, or overheated, material was observed to have a radically different inclusion microstructure. Figure 8 illustrates a typical series of inclusions. The manganese sulfides tended to form this type of array, typical of grain boundary precipitation throughout the sample. The manganese sulfides were identified with the use of an energy dispersive x-ray analyzer. A typical manganese sulfide trace is shown in Figure 9.

The third lot of steel designated as marginal, evinced a microstructure about midway between the two extremes already mentioned. With its marginal rating, this type of structure would be expected. Figure 10 illustrates a typical area in this material. The particles are somewhat random and are not lined up as in the overheated steel. These samples set the standard for the subsequent experiments.

2. Effect of cooling rate and temperature

In most cases, the results were almost identical for each temperature and cooling rate regardless of the lot in this series of experiments. In the cases where differences were significant among the lots, the specifics will be mentioned, otherwise the lots will be grouped together.

The observations of the material overheated at the high end of the overheating range were consistent with what might be expected. The specimen that was oil quenched exhibited the typical microstructure of the clean or non-overheated steels. A comparison of Figure 11 and the previously mentioned Figure 7 illustrates the similarity. The small particles, containing iron, chromium and manganese, are carbides. The air-cooled samples at this and the other temperatures show a microstructure similar to that of the overheated steels. Figure 12 shows the common microstructure comparable to Figure 8. The furnace-cooled samples had a somewhat different microstructure. The inclusion structure typical in the furnace cooled samples is illustrated in Figure 13a. The sulfides tended to be larger and also to cluster more. Figure 13b, illustrating a large central manganese sulfide plus numerous smaller sulfides nearby, shows this type of structure.

Those specimens heat treated in the middle of the overheating range yielded essentially identical results to those just mentioned. In the case of the air-cooled samples, the precipitation was perhaps not as extensive as that found in the samples heat treated at 1375°C, however, the difference was not very great. Otherwise, the observed microstructures paralleled those found in the previous group.

The samples heat treated at the lower extreme of the overheating range produced an interesting result. The air-cooled samples of the three lots did not have the same structure. One of the samples had structures typical of the overheated condition. The other samples had a much cleaner structure, more typical of that illustrated in Figures 7 and 11. The samples that were oil quenched and those that were furnace cooled exhibited the microstructures found in the previous samples treated at the higher temperatures.

The results of this set of experiments on the commercially produced steels is illustrated in Figure 14. This figure shows that overheating is strongly dependent on the cooling rate from the overheating range. The critical cooling rate is approximated by an air cool, approximately 100°C. Cooling rates above and below this critical rate alter the sulfide inclusion distribution such that it takes on relatively harmless forms. (The interior section is, of course, the overheated area.)

B. Altered Chemistries

These samples took on three forms. The first, coded 69, contains very little manganese or silicon. The next specimen, coded 71, contains approximately 1 1/2 weight percent aluminum and silicon. The lot, coded 76, contains about 3 1/2 percent

manganese. The final lot contains 0.012 weight percent cerium and is coded RE. The steels otherwise are nominally AISI 4340. The as-received samples were not investigated since they had not been treated in a uniform manner. The chemistries are listed in Table 2.

1. Low-manganese steel

There were few or no manganese sulfide inclusions present in these steels. However, some particles of various compositions were present. All of the oil quenched samples exhibited the fairly clean microstructure typically found, shown in Figure 7. There were small, random particles which were usually aluminum and iron bearing. These, however were widely scattered. Those specimens that were air-cooled showed a larger number of particles than did the furnace cooled sample. The only difference between the two samples seemed to be in degree. The furnace-cooled samples simply had somewhat larger particles. The differences between samples heat treated at the different temperatures was essentially non-existent. Figure 15 illustrates the typical air-cooled structure. As shown, the particles are fairly small and are well scattered. The furnace-cooled samples are essentially the same. Very few sulfur bearing particles were found. Usually, when particles were found to contain sulfur, it was tied up with iron, titanium, chromium and/or aluminum. On one occasion

a series of small particles was identified as manganese sulfides with significant amounts of chromium included. These particles are shown in Figure 16 and must be considered the exception.

2. High-manganese steel

As usual, the oil-quenched specimens showed little of interest. No sulfur-bearing particles were found. There was however, a random assortment of small and widely spaced alumino-silicates.

In general, the remaining samples did not vary much. All contained a random assortment of alumino-silicates and various other particles. An occasional small iron sulfide particle was identified. The distribution of these particles was very random. Figure 17a illustrates the microstructure found in a typical air-cooled sample. An examination of the small particles dispersed throughout the sample, as shown in Figures 17a and b, revealed that they contained large amounts of iron, manganese and chromium with small amounts of sulfur present. It would seem that the sulfur has been forced to combine with the manganese in the carbides.

3. Aluminum-silicon bearing steel

In the oil quenched samples there were very few particles visible. There were a few randomly scattered

alumino-silicates scattered throughout, however. These were quite random. In general, the samples heat treated at the higher temperatures showed larger particles and they tended to cluster badly. Figure 18 illustrates a typical cluster of alumino-silicates. These particles also contain small amounts of iron. Very few large sulfur bearing particles were identified. On occasion, the alumino-silicates contained very small amounts of sulfur. As with the previous samples, examination of the small round particles revealed the presence of small amounts of sulfur along with large amounts of iron, chromium and manganese. As with the other samples with altered chemistries, there was no evidence of detrimental sulfide precipitation.

4. Rare-earth bearing steel

All of these specimens were air cooled. In comparison with the commercially produced steels, these specimens exhibited a fairly clean microstructure. Those specimens heat treated at the higher temperature 1250°C - 1400°C were lacking any evidence of simple manganese sulfides. The sulfur was tied up in complex cerium bearing particles. In a few instances, iron sulfides were found in conjunction with these complex cerium bearing particles. Figure 19 is a micrograph of a typical section of a sample heat treated at 1350°C. Figure 20 shows an x-ray analysis of a complex

sulfide. A close examination of Figure 19 shows that the particle present formed around a larger pre-existent inclusion that proved too large to be extracted. This was fairly common in these samples.

The samples heat treated at the lower temperatures, 1100°C - 1200°C, exhibited a slightly different microstructure. In general, the sulfur was tied up in the usual complex cerium bearing inclusions, however, there were a few manganese sulfides visible. Usually, these particles did have other elements associated with them. None of the specimens exhibited a "regular" inclusion microstructure. Figure 21 illustrates the typical inclusion microstructure found in these specimens.

V. DISCUSSION

A. Effect of Cooling Rate and Temperature

During the examination of the various specimens it became obvious that the cooling rate was indeed a critical factor for producing the overheated inclusion structure. High cooling rates, like those found in an oil quench, produce a microstructure free of detrimental sulfide arrays. At overheating temperatures, the sulfides tend to dissolve and enter into solid solution with the austenite. The subsequent cooling rate is fast enough to freeze the sulfides into the matrix. Any precipitation that happens after this step will not occur in a regular array on grain boundaries and thus will not be as detrimental to the materials' mechanical properties.

At the critical cooling rate, however, the sulfides are able to precipitate onto the high temperature austenitic grain boundaries. The kinetic forces governing precipitation are balanced at this point. The cooling rate is slow enough to allow precipitation to occur at the preferred nucleation sites, the austenitic grain boundaries, but fast enough to prevent any extensive ripening of the sulfides. The result is that a large number of very small manganese sulfides form an almost continuous network in the material. The fracture, at room temperature is actually transgranular through the

existing grains but is intergranular if the austenitic grains are used as the reference point.

The lower cooling rate of the furnace cool offers another solution to the overheating problem. The sulfides are allowed to precipitate onto the grain boundaries but, in this case, the thermal driving force for growth is large enough to promote extensive ripening of the sulfides. Examination of the respective figures support these findings. The furnace cooled samples exhibit fewer but larger manganese sulfides than the air cooled samples whereas the oil quenched samples showed few, if any small particles.

In this series of experiments, the temperature did not play a large part in the overheating process. It can be assumed that the overheating onset temperature (OOT) was somewhere above 1100°C for these samples. The one exception would be for the sample designated L3. The other specimens exhibited a superior structure when air cooled from 1100°C. This would seem to indicate a higher OOT. Examination of the data shows that the sample known as L3 has a lower sulfur content than do the others. This would seem to support the previous findings that the sulfur level and the OOT increase together. Thus it can be seen that the OOT is indeed a characteristic property of each steel, dependent at least partially on the sulfur

content. Interactions between the various other components of the steel could cause other variations in the overheating onset temperature.

B. Effects of Chemistry Changes

1. Low-manganese steel

A decrease in the manganese content of a steel has been found to increase the solubility of sulfides in austenite. Figure 22 illustrates the interaction between manganese and sulfur in austenite. Lowering the manganese would seem to have two positive effects for the prevention of overheating. First, of course, the removal of the manganese itself. This reduces the amount of manganese sulfide available for precipitation. Second is the increase in sulfur solubility. The driving force for sulfide precipitation would be reduced by this effect. Manganese does play an important part in the hardenability of the steel. However, there are other considerations. The examination of this steel, with Figure 14 as an example, does show that the material is totally free of inclusion problems. The actual effects on processing and material properties would have to be examined.

2. High-manganese steel

An increase in the manganese content has the opposite effect on the solubility of sulfur in austenite as seen in

Figure 18. The majority of the sulfides could not go into solution; thus, at overheating temperatures, the driving force for sulfide growth would be very high. One would expect to find an occasional large sulfide with some minor grain boundary precipitation. The examination of this steel seems to favor this conclusion. On very rare occasions a manganese sulfide was identified. However, the majority of the particles contained iron, aluminum and silicon. As always there are problems associated with an increased manganese content. It has been found that excessive amounts of manganese can lead to temper embrittlement.

3. Aluminum-silicon bearing steel

It has been suggested that an increase in the aluminum content of steel would have the opposite effect on the solubility of sulfides that manganese does. Whereas manganese decreases the solubility, it is expected that aluminum would increase it. It could be assumed from the observations that this premise was correct. Very few sulfur bearing particles were identified. In only one case was a manganese sulfide found. It would seem that the addition of aluminum was an effective method for removing sulfides. However, there is the difficulty caused by an increased number of alumino-silicates present. A study to determine the effect of these particles would have to be launched before this method of

overheating prevention could be instituted.

4. Rare-earth bearing steels

The addition of rare-earth elements such as cerium and lanthanum creates a thermodynamically feasible substitution for manganese in sulfides. The rare-earth elements combine with the sulfur and oxygen present in the steel to form complex sulfides and oxysulfides. These particles tend to be stable at high temperatures and grow rather than to go into solution. The figures illustrating these specimens, Figures 19 and 21, show the image of a large particle that was not removed from the matrix material. X-ray analysis of the surrounding areas show evidence that this large particle was also a rare-earth bearing inclusion through trace amounts left in the surrounding carbon support structure. It would seem that, from the results obtained, that the addition of rare-earth elements is a feasible method of eliminating the sulfide problem.

VI. CONCLUSIONS

Electron microscopy was used to investigate the behavior of manganese sulfides in electroslag remelted steels. Different process steps and chemistry alterations were made in an attempt to eliminate or change the sulfide distribution that leads to overheating. The following conclusions were made:

1. Precipitation of manganese sulfides onto high-temperature austenitic grain boundaries is directly responsible for overheating as evidenced through previous work and the results of the initial study on the as-received steels.

2. The critical step in the overheating process is the cooling rate from the overheating range, 1100°C - 1400°C. The critical cooling rate approximates an air cool, about 100 °C/minute.

3. A high cooling rate eliminates overheating by "freezing" the sulfur in solution. A low cooling rate enhances ripening of the sulfides. The larger, clustered sulfides do not cause a deterioration in mechanical properties.

4. The simplest method for the elimination of detrimental manganese sulfide inclusions is to alter the cooling rate after high temperature thermo-mechanical treatment.

5. The alternative method of eliminating sulfide precipitation leading to overheating is to alter the chemistry of the steel.

6. A decrease in the manganese content of the steel increases the solubility of sulfur in austenite. This results in a decrease in the amount available for precipitation.

7. An increase in the manganese content decreases the solubility of sulfur in austenite. The manganese sulfides thus will ripen upon heat treatment at high temperatures and will not precipitate upon cooling.

8. The addition of aluminum seems to affect sulfur solubility in the same manner as a decrease in the manganese content. The solubility of sulfur increases, promoting retention of the sulfur in solid solution.

9. The addition of rare-earth elements such as cerium creates a substitution such that stable cerium sulfides are formed.

10. In the cases of increased sulfur solubility, there is a driving force for the pickup of sulfur into the metallic carbide phase.

Much remains to be investigated in the behavior of sulfur with respect to chemistry changes in steel. A special interest in the effects of these changes on mechanical properties is necessary.

APPENDIX - Carbon Extraction Replication

Carbon extraction replicas are used in the electron microscopic examination of multi-phase systems in which the matrix is chemically anodic to any precipitate found in it. The process for making extraction replicas is as follows [31].

1. A polished and lightly etched sample is placed in an evaporating unit. A carbon film is then formed on the surface by resistance heating a carbon rod. The film thickness is estimated by the color change of the specimen surface.

2. The film is stripped from the sample by immersing in a suitable medium, 5 - 10% Nital for the steels in this study.

3. The specimen is dipped into distilled water where surface tension effects cause the film to float. The film breaks up into pieces suitable for capture on copper grids for microscopic examination. These are the extraction replicas.

This process enables the researcher to examine the inclusion structure without interference from the matrix. This is particularly advantageous in steels. The magnetic

properties inherent in the iron matrix can cause bending in the electron beam of a microscope. This system facilitates the examination of particles by x-ray analysis by eliminating spurious matrix effects.

BIBLIOGRAPHY

1. A. Preece, A. Hartley, S. E. Mayer and J. Nutting, "The Overheating and Burning of Steel," JISI, 153, 237 (1946).

2. W. E. Goodrich, "Overheating and Burning of Nickel-Chromium-Molybdenum Steel", JISI, 153, 255 (1946).

3. J. Woolman and H. W. Kirkby, "Some Experiments on Overheating", JISI, 153, 265 (1946).

4. A. Preece, J. Nutting and A. Hartley, "The Overheating and Burning of Steel," JISI, 164 37 (1950).

5. T. Ko and D. Hanson, "Grain-Boundary Phenomena in Severely Heated Steel", JISI, 164, 51 (1950).

6. E. C. Rollason and D. F. T. Roberts, "A Note on the Overheating of Steel", JISI, 164, 422 (1950).

7. A. Preece and J. Nutting, "The Detection of Overheating and Burning in Steel by Microscopical Methods", JISI, 164, 46 (1950).

8. I. S. Brammar, "A New Examination of the Phenomena of Overheating and Burning of Steels", JISI, 201, 752 (1963).

9. I. S. Brammar and R. W. K. Honeycombe, "Intergranular Brittleness of Cast Chromium-Nickel Steels", JISI, 200, 1060 (1962).

10. G. D. Joy and J. Nutting, "Effect of Second-Phase Particles on the Mechanical Properties of Steel", The Iron and Steel Institute, London, 95 (1971).

11. T. J. Baker and R. Johnson, "Overheating and Fracture Toughness", JISI, 211, 783 (1973).

12. R. O. Ritchie and J. F. Knott, "On the Influence of High Austenitizing Temperatures and 'Overheating' on Fracture and Fatigue Crack Propagation in a Low Alloy Steel", Met. Trans., 5, 782 (March 1974).

13. T. J. Baker and W. D. Harrison, "Overheating and Burning in Steel Castings", Met. Tech., 2, 201 (May 1975).

14. D. R. Glue, C. H. Jones and H. K. M. Lloyd, "Effect of Composition and Thermal Treatment on the Overheating Characteristics of Low-Alloy Steels", Met. Tech., 9, 416 (September 1975).

15. R. C. Andrew, G. M. Weston and R. T. Southin, "Overheating in Low Sulfur Steels", J. Austrailian Inst. Metals, 21, 126 (1976).

16. R. C. Andrew and G. M. Weston, "Formation of Cratered Overheating Facets", Metals Science, 142 (April 1977).

17. R. C. Andrew and G. M. Weston, "The Effect of Overheating on the Toughness of Low Sulfer ESR Steel", Metals 77, 30th Annual Conference of the Austrailian Institute of Metals, Newcastle (May 1977).

18. R. C. Andrew and G. M. Weston, "The Effect of the Interaction between Overheating and Tempering Temperature on the Notch Toughness of Two Low Sulfer Steels", J. Austrailian Inst. Metals, 22, 200 (September 1977).

19. J. Nutting, Seminar given at AMMRC, Watertown, Massachusetts (July 25, 1978).

20. H. E. McGannon, ed., The Making, Shaping and Treating of Steel, 9th edition (1971), United States Steel Corporation.

21. J. Nutting, "The Precipitation of MnS from Austenite", Physical Chemistry in Metallurgy, Proceedings of the Darken Conference, U.S.S. Research Laboratory, Monroeville, Pennsylvania (August 1976).

22. K. Schwerdtfeger, "Sulfide Formation in Low Alloyed Steel", ibid., 229.

23. T. J. Baker and J. A. Charles, "Morphology of Manganese Sulfide in Steel", JISI, 210, 702 (September 1972).

24. L. K. Bigelow and M. C. Flemings, "Sulfide Inclusions in Steel", Met. Trans., 6B, 275 (June 1975).

25. Luycks, J. R. Bell. A. McLean and M. Korchynsky, "Sulfide Shape Control in High Strength Low Alloy Steels," Met. Trans., 1, 3341 (December 1970).

26. J. H. Little and W. J. M. Henderson, "Effect of Sulfide Inclusions on the Anisotropy of Ductile Charpy Shelf Energy", Proceedings of a Conference Organized by the Corporate Laboratory of the BSC and the ISI (24-25 March, 1971).

27. B. J. Schultz and C. J. McMahon, Jr., "Fracture of Alloy Steels by Intergranular Microvoid Coalesence as Influenced by Composition and Heat Treatment", Met. Trans., 4, 2485 (October 1973).

28. L. H. Van Vlack, ed., "Oxide Inclusions in Steel", International Met. Treview, 187 (September 1977).

29. K. Narita, "Observation, Identification and Determination of Nonmetallic Inclusion and Precipitate in Steel", Trans. ISIJ, 16, 208 (1976).

30. T. Fujii, D. R. Poirier, and M. C. Flemings, "Coarsening Kinetics of Second Phase Particles", to be published.

31. G. Thomas, Microscopy of Metals, (1962), John Wiley and Sons, Inc.

Figure 1 Typical faceted overheating fracture, 9.4X.

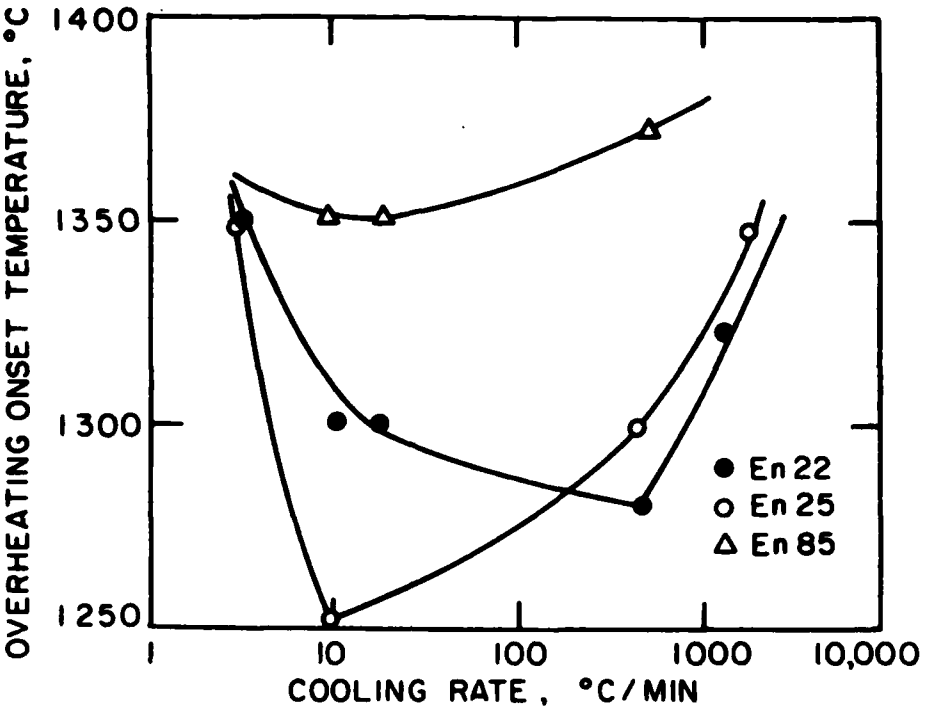

FIGURE 2 EFFECT OF COOLING RATE ON OVERHEATING TEMPERATURE. (REFERENCE 4)

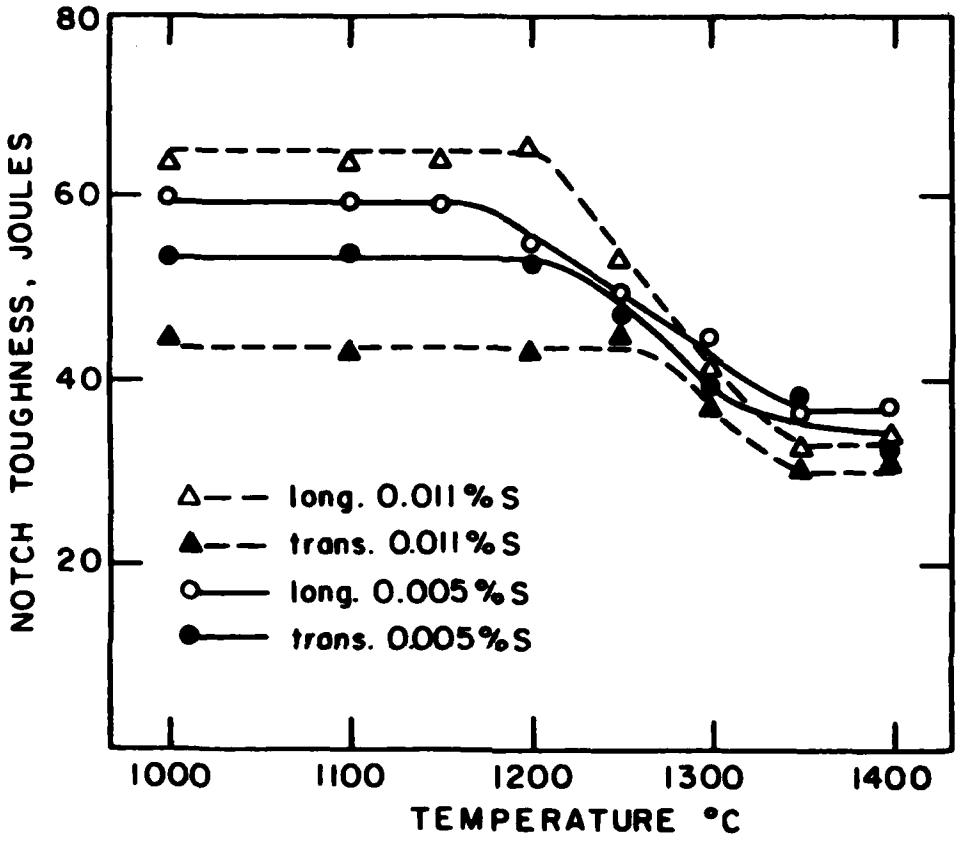

FIGURE 3 EFFECT OF HEATING TEMPERATURE ON THE NOTCH TOUGHNESS OF TWO ESR STEELS. (REFERENCE 17.)

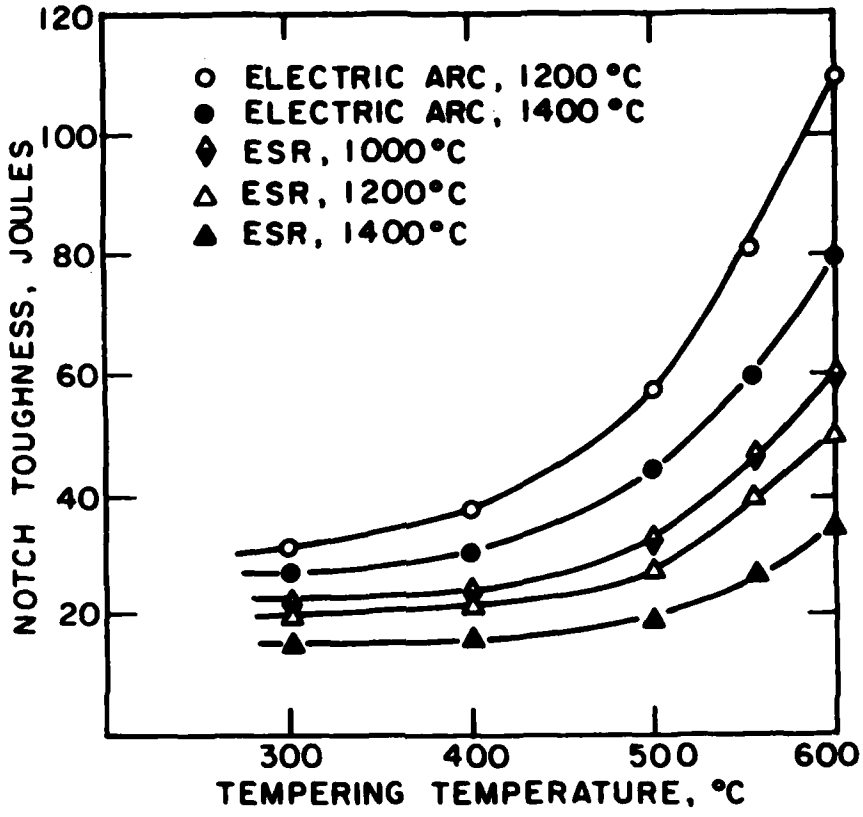

FIGURE 4 LONGITUDINAL ROOM-TEMPERATURE NOTCH IMPACT TOUGHNESS OF TWO LOW SULFUR STEELS HEATED AT THE TEMPERATURES SHOWN AND THEN TEMPERED IN THE RANGE 300-500°C. (REFERENCE 18)

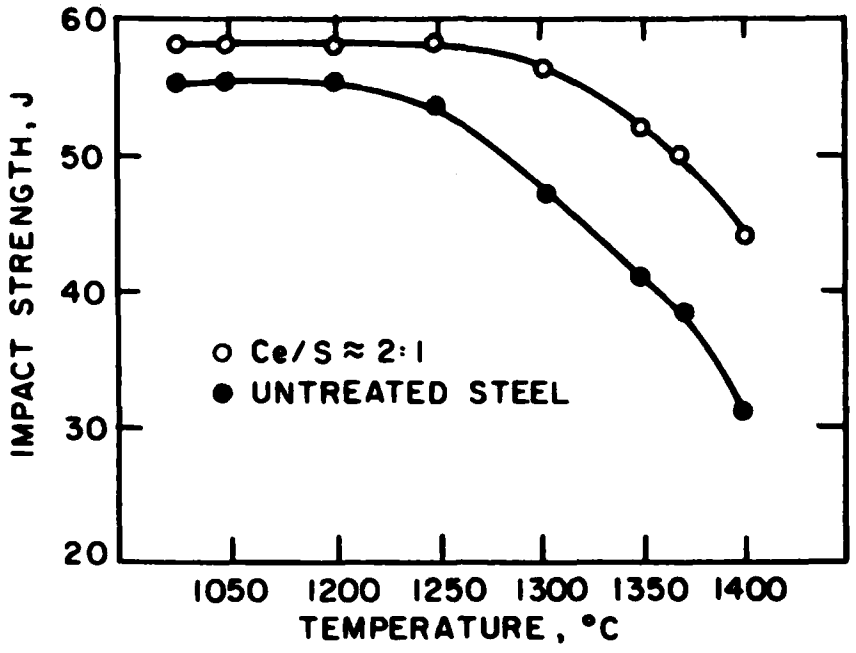

FIGURE 6 EFFECT OF AUSTENITIZING TEMPERATURE ON IMPACT TOUGHNESS OF RARE-EARTH TREATED + UNTREATED STEELS. (REFERENCE 14)

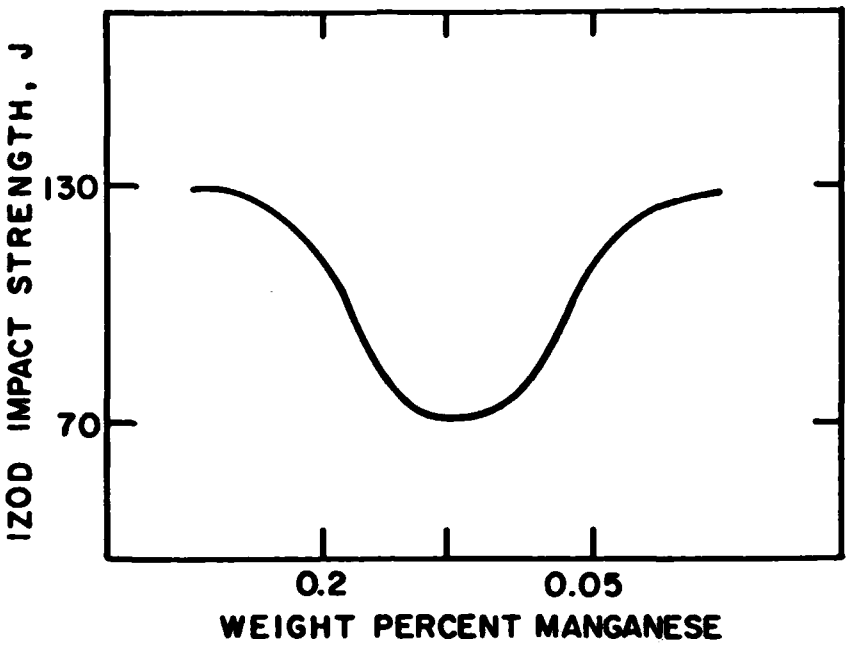

FIGURE 5 EFFECT OF MANGANESE CONTENT ON THE IZOD IMPACT STRENGTH OF A STEEL TREATED IN THE OVERHEATING RANGE. (REFERENCE 19)

Figure 7 Carbon extraction replica of a 4340 steel treated in the overheating range but showing an acceptable condition, 5000X.

Figure 8 Carbon extraction replica of a 4340 steel exhibiting an overheated inclusion structure, 5000X.

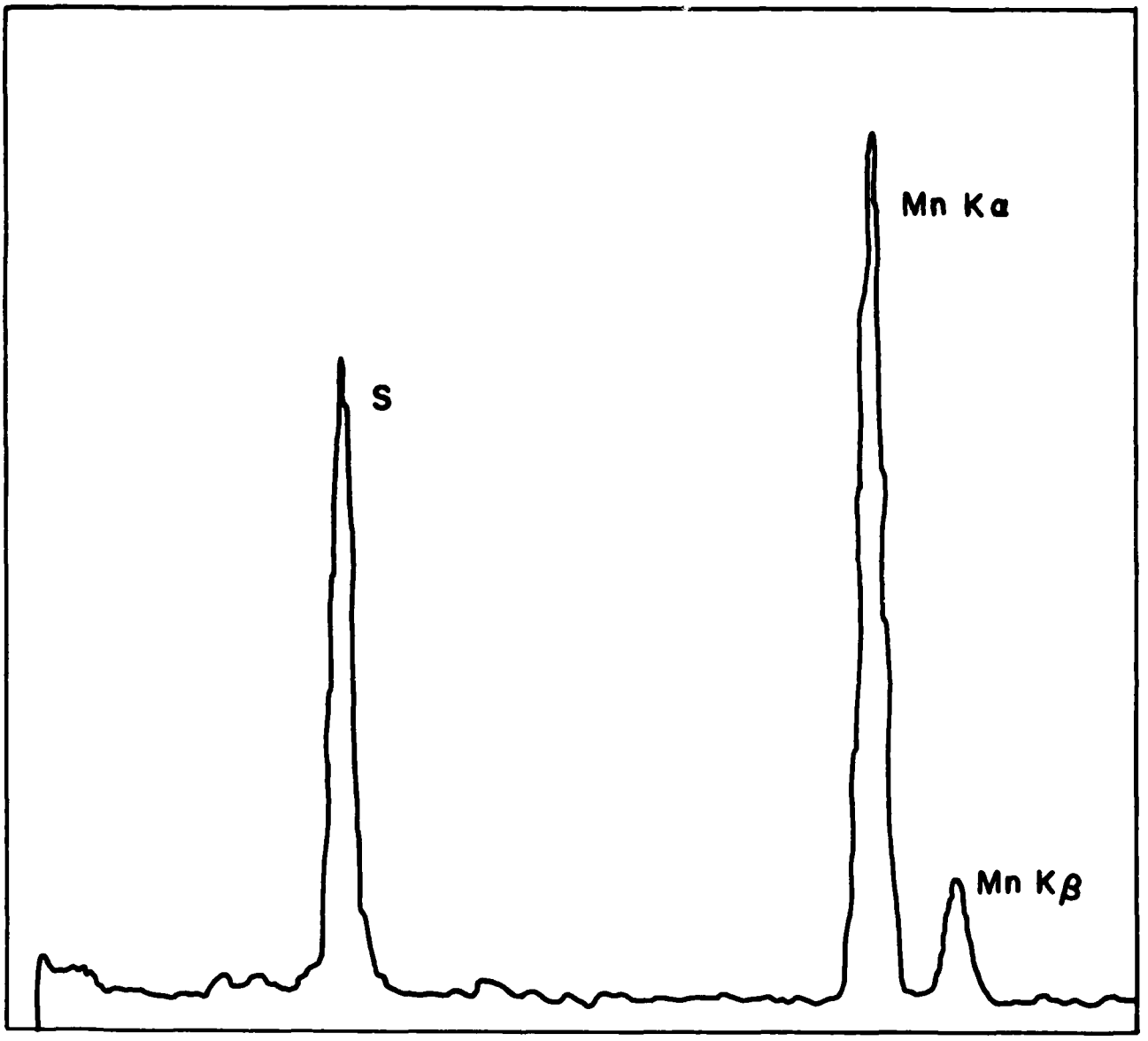

FIGURE 9 SPECTRUM SHOWING X-RAY ANALYSIS OF A MANGANESE SULFIDE PARTICLE

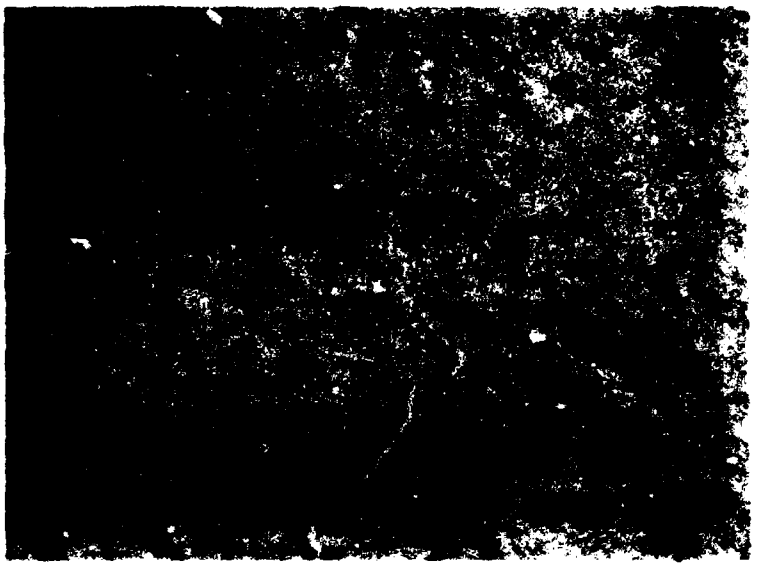

Figure 10 Carbon extraction replica of a 4340 steel exhibiting a marginally acceptable inclusion structure, 2000X.

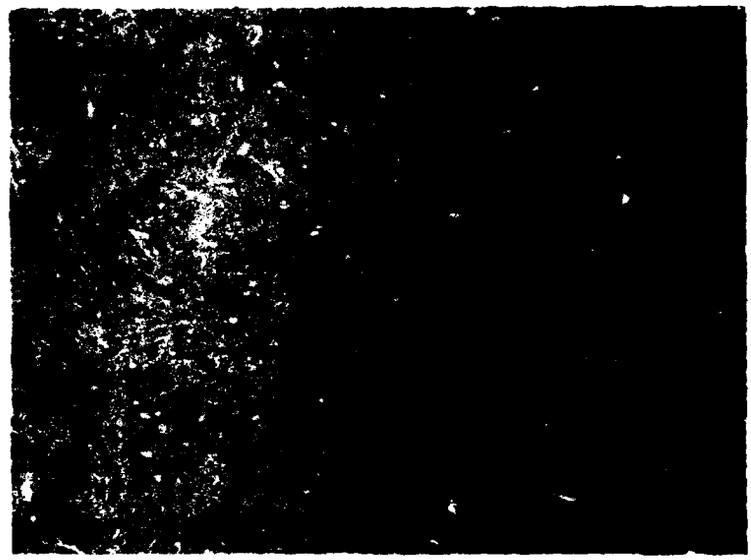

Figure 11 Carbon extraction replica of a steel oil quenched from within the overheating range, 5000X

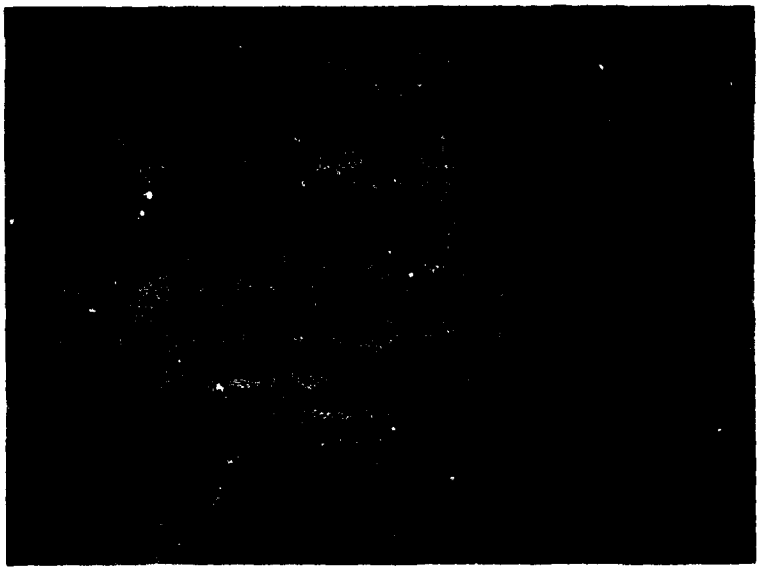

Figure 12 Carbon extraction replica of a steel air cooled through the overheating range, 5000X.

(a) (b)

Figure 13 Carbon extraction replicas of a 4340 steel, furnace cooled through the overheating range; (a)manganese sulfide group, 10,000X and (b)central sulfide with surrounding smaller sulfides, 10,000X.

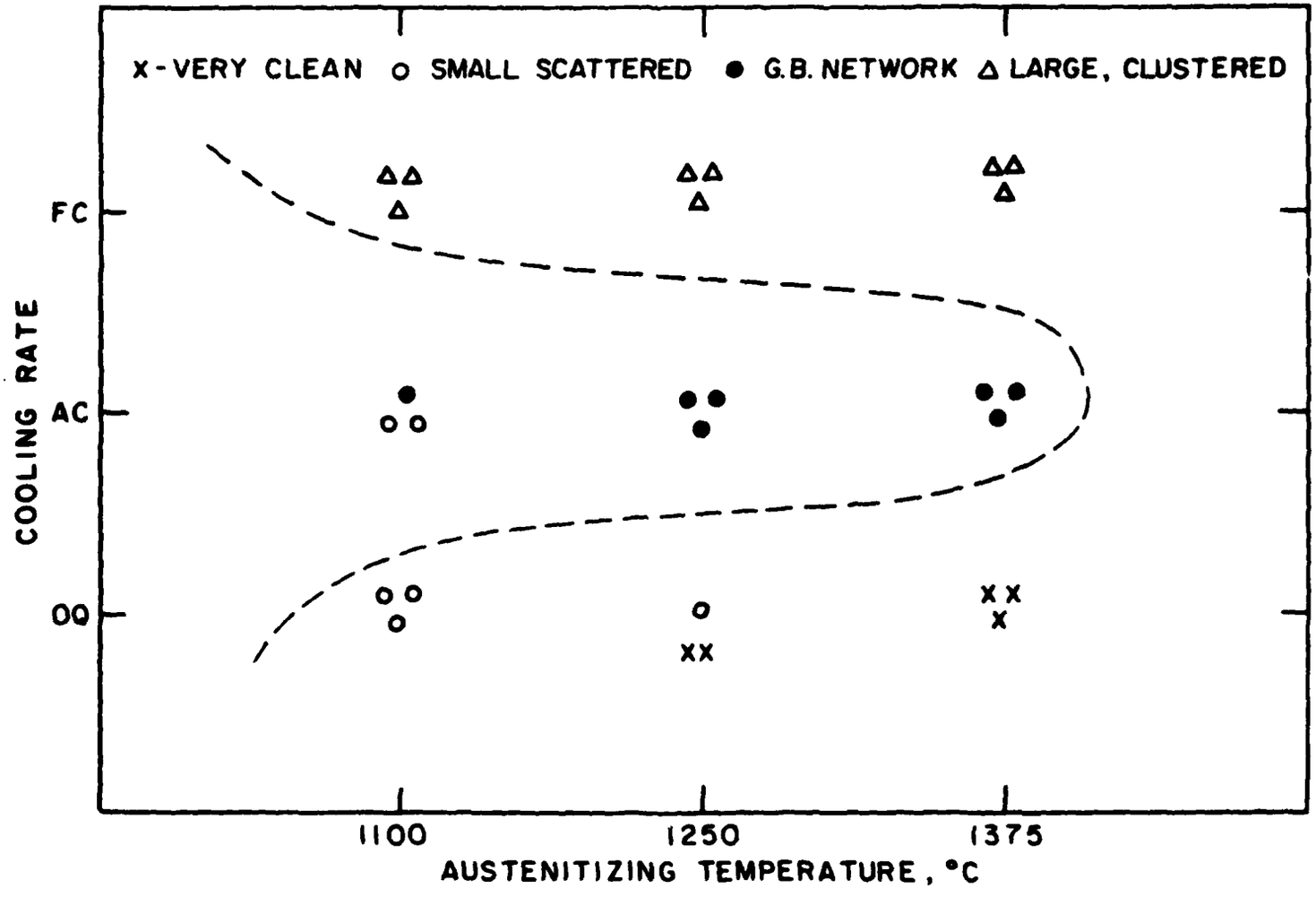

FIGURE 14 MAP OF INCLUSION DISTRIBUTION IN COMMERCIALLY PRODUCED STEELS AFTER HEAT TREATMENT

Figure 15 Carbon extraction replica of a nominal 4340 steel with low manganese after heat treatment at 1100°C and a furnace cool, 5000X.

Figure 16 Carbon extraction replica of the low manganese steel showing small manganese sulfides, 10,000X.

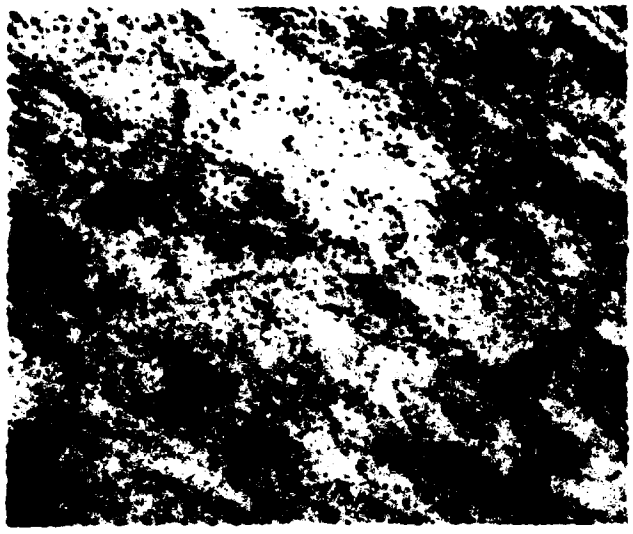

(a)

(b)

Figure 17 Carbon extraction replica of a high manganese steel after heat treatment at 1250° and an air cool; (a)Iron, aluminum and silicon bearing particles, 10,000X and (b)Sulfur bearing carbide containing iron, chromium and manganese, 200,000X.

Figure 18 Carbon extraction replica of an aluminum-silicon bearing steel after heat treatment at 1250°C and an air cool, 2000X.

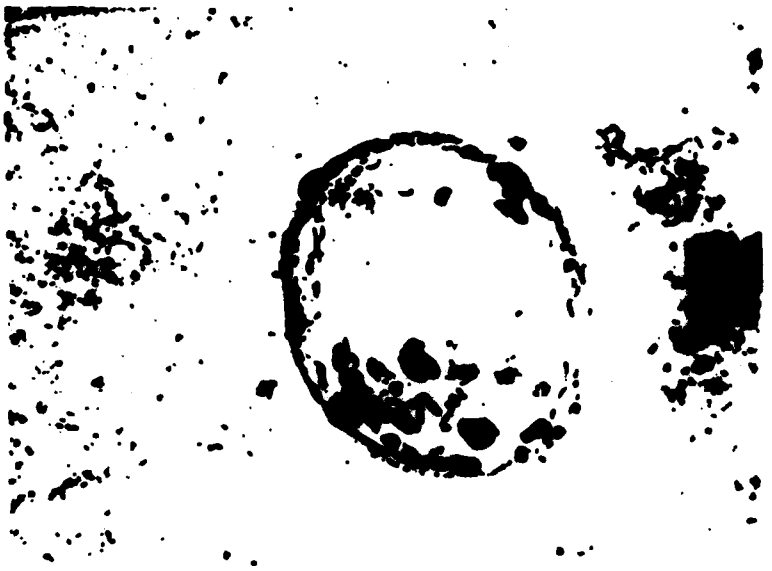

Figure 19 Carbon extraction replica of a rare earth bearing steel after heat treatment at 1300°C and an air cool, 20,000X.

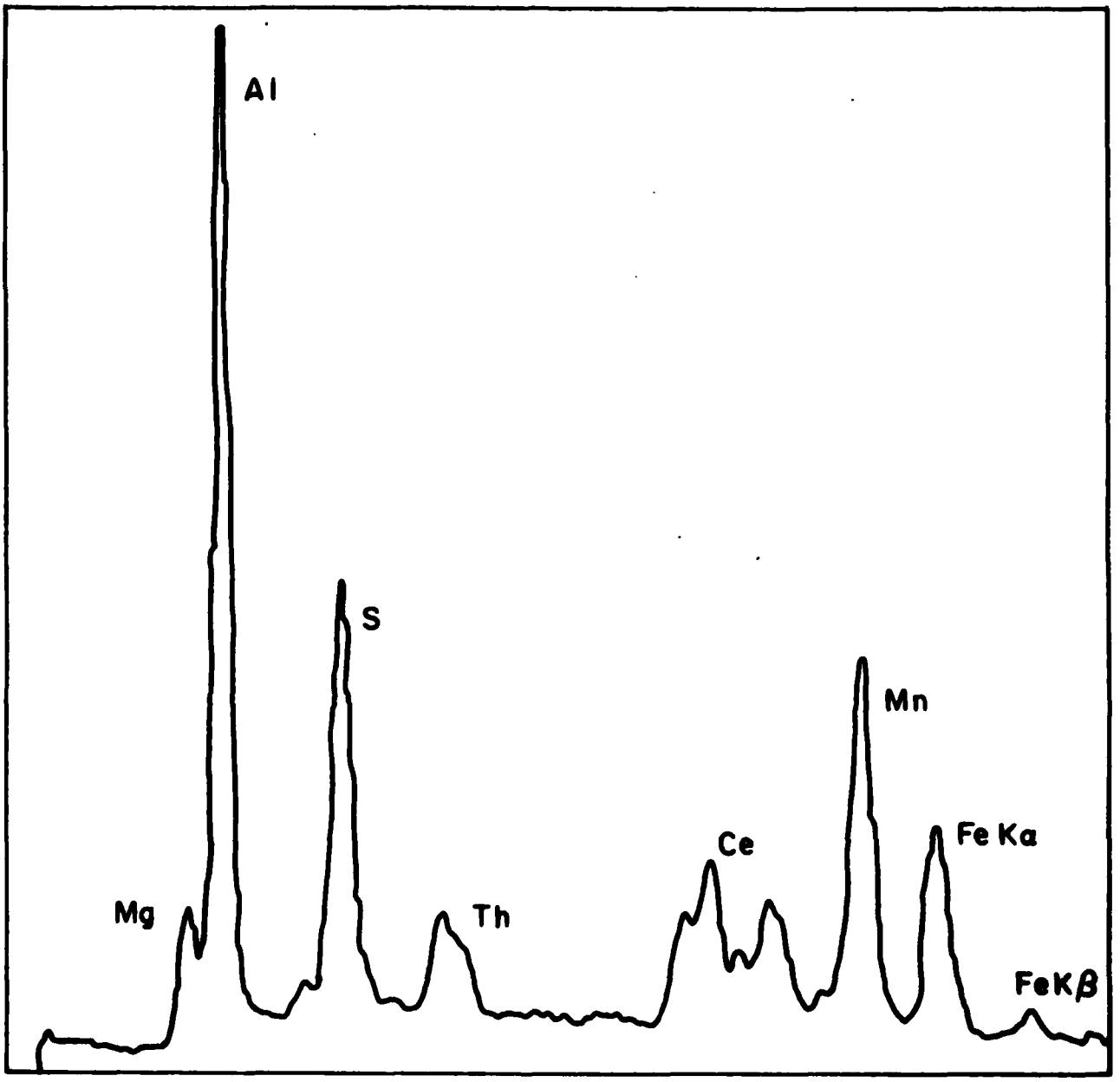

FIGURE 20 SPECTRUM SHOWING X-RAY ANALYSIS OF A COMPLEX CERIUM-BEARING SULFIDE

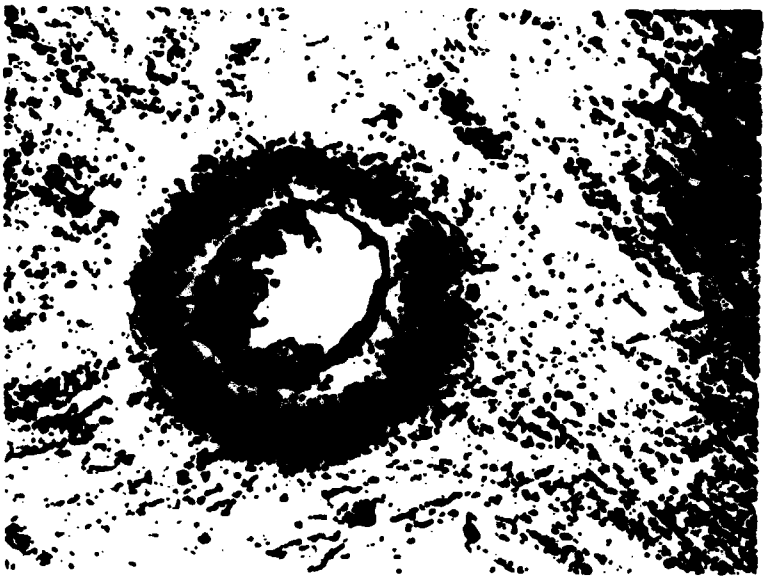

Figure 21 Carbon extraction replica of a rare earth bearing steel heat treated at 1050°C and air cooled, 10,000X.

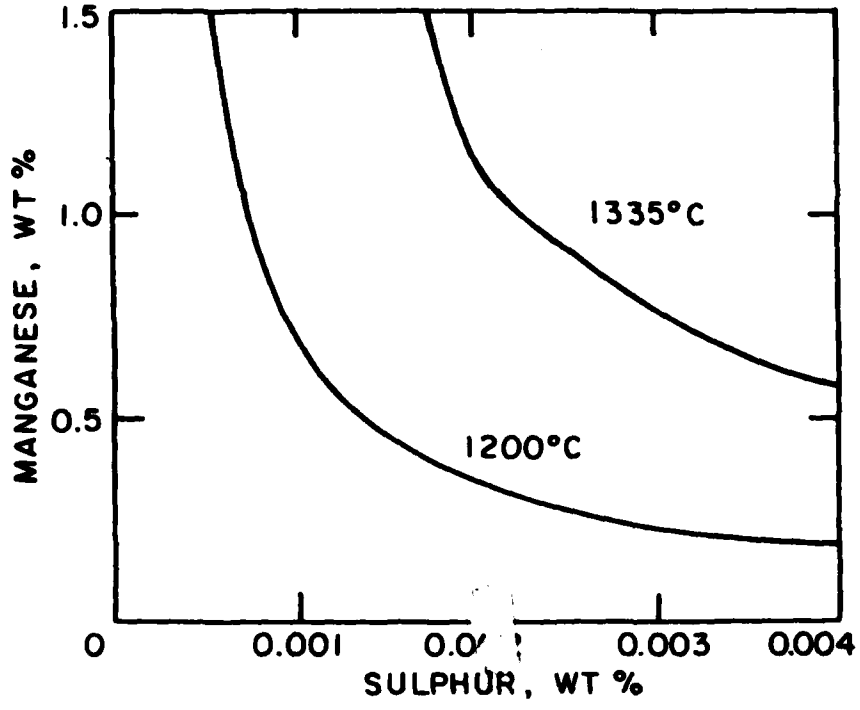

FIGURE 22 MANGANESE AND SULFUR SOLUBILITY IN IRON (REFERENCE 20)

PART II. COARSENING KINETICS OF SECOND PHASE PARTICLES

I. SUMMARY

A model to simulate the diffusion-controlled coarsening and dissolution kinetics of particles within a metallic matrix is formulated. With an arbitrary size distribution of particles, the model can be used to calculate the change in the size distribution of particles during coarsening or dissolution. Other system parameters, such as average radius of particles, volume fraction, average distance between particles, surface area, and matrix composition are also calculated. An important result is that kinetics do not generally obey the often-applied Lifshitz -Slyozov-Wagner theory for diffusion controlled coarsening based upon concentration profiles around isolated spheres. In such a formulation, the direct effect of the surrounding particles is neglected. In our model, which is a modification of the coarsening kinetics described by Weins and Cahn, the effect of surrounding particles is incorporated because the system is taken to be a system of point potentials, each with a potential according to its radius or curvature.

Calculations are on silica particles in a copper matrix and on manganese sulfide inclusions in iron, with emphasis on the latter, in order to predict their behavior during homogenization or soaking treatments. The effect of composition

of manganese, from 0.1 to 1.2 percent, on the coarsening of sulfides in a "high" sulfur (0.017 percent) steel and a "low" sulfur (0.003 percent) steel was investigated. As expected, manganese strongly reduces the rate of coarsening, particularly for times of ten hours or less in the temperature range of 1100°C - 1400°C.

Calculated results also indicate that the rate of dissolution at temperatures greater than the solvus for manganese sulfide inclusions in austenite is very low.

II. INTRODUCTION

Relationships to describe the kinetics of growth and dissolution and coarsening of second phase particles have been derived by many workers. Their contributions can be classified into the following groups:

1. dissolution or growth of a single particle [1-4],
2. dissolution or growth of particles within a group assuming no interaction among the diffusion fields surrounding each particle [5-8],
3. dissolution or growth of particles within a group considering one dimensional and linear solute distribution in the matrix between nearby particles [9,10], and
4. the growth of particles within a group of particles considering each particle as a point potential in a diffusion field which satisfies the LaPlace equation [11,12].

In the second group, previous workers have derived the following equation to describe coarsening:

$$\bar{R}^3 - \bar{R}_o^3 = \frac{8\ DC_{eq}\sigma V_m^2}{9\ R_g T} \qquad (1)$$

where $\bar{R}^3$ and $\bar{R}_o$ are the average radii of inclusions at time t and zero time, respectively; D is diffusivity; C_{eq} is the solubility in the matrix; σ is the particle-matrix interfacial energy; V_m is the molar volume; R_g is the gas content and T is absolute temperature. Equation (1) is called the Lifshitz Slyozov-Wagner theory (i.e., L.S.W. theory) and has been applied to the coarsening of precipitates in some binary metallic systems [13,14] where the kinetics of coarsening are limited by diffusion through the matrix. Calculations of particle sizes using the L.S.W. theory have also been compared to measurements of the coarsening of silica in copper [15].

Included among the third group is the expression given by Greenwood [9] who considered a system of N particles, in which the growth of a particle of radius R is given by

$$4\pi\rho R^2 \frac{dR}{dt} = DC_{eq} \frac{2V_m\sigma}{R_g T} \sum_{i=1}^{N} \left(\frac{A}{x}\right)_i \left(\frac{1}{R_i} - \frac{1}{R}\right) \qquad (2)$$

where ρ is the density, R_i is the radius of the i-th particle, and $(A/x)_i$ is the area-to-length ratio of the effective diffusion path between the particles with radii R and R_i. The basic concept behind Equation (2) is that there is one-dimensional (non-radial) steady state diffusion between any two particles each with a potential given by the Thomson-Freundlich equation according to their respective radii.

Weins and Cahn [11,12] pointed out a number of difficulties with Equation (2). The most serious drawback is that one-dimensional flow does not, in fact, describe diffusion between particles in three-dimensional space, and so the effective area-to-length ratio cannot be evaluated. They give an alternative approach in which the particles are taken to be point potentials for diffusion distributed throughout space, with potentials given by the Thomson-Freundlich equation, and the solute distribution satisfies the Laplace equation. We classify their approach as the fourth group above.

In this paper we use the basic approach of Weins and Cahn [11,12], except that we apply it to a system of a very large number of particles with a known size distribution. In their work, the basic equations were applied to a small number of particles because their intent was to show how kinetics of coarsening phenomena can depend upon specific spatial arrangements of particles. Our calculations permit us to estimate not only the change of average radius with time, but also the change of size distribution. Additionally, average interparticle spacing, specific surface area of particles, volume fraction, and matrix composition are also computed.

First, calculated results are compared with experimental results reported in the literature [15] for coarsening of

silica inclusions in a copper matrix. Second, we compare the model to the experimental results for sulfide inclusions in AISI 4340 low alloy steel [16] containing 0.017% S. Finally, using the model, predictions are made on the ripening and dissolution kinetics of MnS inclusions in both "low" sulfur steel (0.003% S) and "high" sulfur steel (0.017% S) during high temperature homogenization and soaking treatments for hot working.

III. DIFFUSION MODEL

The kinetics of coarsening and dissolution are given in terms of the time rate of change of the size distribution of particles within the system. The kinetics can be limited either by the diffusion of material through the matrix from the dissolving to the growing particles, or by the reaction at the particle-matrix interface. According to previous workers, the ripening of sulfide inclusions in steel is limited by diffusion [16,17] in the same way as the ripening kinetics of many oxide particles in metals.

The time and spatial variation of concentration in the matrix is given by

$$\frac{\partial C}{\partial t} = D\nabla^2 C \qquad (3)$$

where C and t are concentration and time and D is diffusion coefficient. During homogenization, matrix composition changes very slowly with time. Then we neglect $\partial C/\partial t$ in Equation (3) so that

$$\nabla^2 C = 0 \qquad (4)$$

The matrix composition at the particle surface is given by

the Thomson-Freundlich equation which accounts for the effect of curvature on solubility limit. The equation can be expanded in a Taylor series and then written in the following approximate form:

$$C_i = C_{eq} + \frac{\Gamma}{R_i} \qquad (5)$$

where, $\Gamma = 2\sigma V_m C_{eq}/R_g T$ and C_i is the matrix composition at the surface of a particle with a radius, R_i. The error introduced by the Taylor series approximation is about 5 percent in the value of C_i given by Equation (5) when applied to silica particles in a copper matrix. For manganese sulfide inclusions in steel, the error is less than 0.2 percent.

Given N particles dispersed in the matrix, whose positions are defined by vectors $\underset{\sim}{r}_j$ (j = 1,....N), and the particles are point sources for diffusion, then the following equation can be obtained as a solution Equation (4) for the concentration distribution in the matrix [11]:

$$C(\underset{\sim}{r}) = C_b + \sum_{j=1}^{N} \frac{M_j}{|\underset{\sim}{r} - \underset{\sim}{r}_j|} \qquad (6)$$

where $C(\underset{\sim}{r})$ is the concentration in the matrix at the position defined by the vector $\underset{\sim}{r}$, M_j is a constant associated with the j-th particle and is defined later, and C_b is the matrix

concentration far from the particles.

M_j must be determined to satisfy the boundary condition of Equation (5) as follows. The average concentration on the surface of the i-th particle, $\bar{C}_i$ is:

$$\bar{C}_i = \frac{1}{S_i} \int_{S_i} \left(C_b + \sum_{j=1}^{N} \frac{M_j}{|\underset{\sim}{r}_{ij} - \underset{\sim}{r}_i|} \right) dS \quad (7)$$

where $\underset{\sim}{r}_{ij}$ is the vector from the i-th particle to the j-th particle, $\underset{\sim}{r}_i$ is vector which defines the surface of the i-th particle, S_i is surface area of the i-th particle and dS is the differential surface element of the i-th particle.

Integration of Equation (7) yields [11]:

$$\bar{C}_i = C_b + \frac{M_i}{R_i} + \sum_{j=1}^{N} \frac{M_j}{r_{ij}} \quad (8)$$

where r_{ij} is the distance between the i-th particle and the j-th particle. Here, we assume the average surface concentration to be equal to the surface concentration obtained in Equation (5). Then,

$$\sum_{j=1}^{N} \frac{M_j}{r_{ij}} = \frac{1}{R_i} \left(\Gamma - M_i \right) + C_{eq} - C_b \quad (9)$$

Similar equations can be written for all particles, i.e., i = 1,2,.....N. Thus, the values of M_j (j = 1,2,....N) are determined by solving these N algebraic equations.

The rate of change of radius of the i-th particle can be determined as follows. A mass balance at the interface between particle and matrix is written as

$$4\pi R_i^2 \left(C_p - C_i\right) \frac{dR_i}{dt} = D \int_{Si} \nabla C_i \cdot \underset{\sim}{n} dS \qquad (10)$$

where, $\underset{\sim}{n}$ is a unit vector normal to the surface of the particle, and C_p is the composition in the particle. Substitution of Equation (6) into Equation (10) and integration using the divergence theorem yields [11]:

$$\frac{dR_i}{dt} = - \frac{DM_i}{R_i^2(C_p - C_i)} \qquad (11)$$

Equation (11) gives the rate of change of the radius of the i-th particle using the value of M_i determined as described above.

Up to this point, the analysis is similar to that of Weins and Cahn [11,12] with the additional assumption that the total volume of particles is kept constant during

coarsening. They applied the model to Ni_3Al particles in a Ni matrix to show the environmental effects on the coarsening kinetics considering 10 to 20 particles dispersed in three-dimensional space. Here we consider a system of a large number of particles of nonuniform sizes in order to relax the limitation of the model regarding the maximum number of particles. This is done by introducing a particle distribution function which is described below.

Start at any point in a sample ($r = 0$) and count the number of particles within a sphere of radius r; let this number be N(r). If the total volume of the sample under consideration is a sphere with radius r_o, then $N(r_o)$ is N, the total number of particles. Thus the fraction of all inclusions in the total volume enclosed by radius r is $N(r)/N(r_o)$. We define the space distribution function, q(r) such that

$$\int_0^r q(r)dr = \frac{N(r)}{N(r_o)} \qquad (12)$$

When $r = r_o$, $N(r)/N(r_o) = 1$ so that q(r) must satisfy

$$\int_0^{r_o} q(r)dr = 1 \qquad (13)$$

q(r), itself, depends upon the manner in which particles are distributed throughout the sample. For a uniform distribution, the R.H.S. of Equation (12) equals the ratio of the volume of a sphere with radius r to the sphere or radius r_o. Thus

$$\int_o^r q(r)dr = \frac{r^3}{r_o^3} \tag{14}$$

so that in order to satisfy Equations (13) and (14) the space distribution function must be

$$q(r) = \frac{4\pi r^2}{V_o} \tag{15}$$

in which V_o is the volume of the sphere with radius r_o.

To completely describe the system of particles we need to describe their size distribution as well as their space distribution. The particles range in size up to a maximum radius of R_M. The size distribution function, f(R), is defined such that

$$\int_o^{R_M} f(R)dR = N(r_o, R_M) \tag{16}$$

where $N(r_o, R_M)$ is the total number of particles of all sizes

in the system with volume V_o. Then the number of particles in the sphere of radius r is

$$N(r,R_M) = \int_o^r \int_o^{R_M} f(R)q(r)dRdr \qquad (17)$$

according to the definition of the space distribution function, Equation (12). Similarly, the number of inclusions with radius R or less and in the entire system is

$$N(r_o,R) = \int_o^R f(R)dR \quad .$$

Finally, the number of inclusions with radius R or less and within the sphere r is

$$N(r,R) = \int_o^r \int_o^R f(R)q(r)dRdr \quad . \qquad (18)$$

Since Equation (18) gives the accumulated number of inclusions, then

$$P(R,r) = f(R)q(r)dRdr \qquad (19)$$

is the number of particles located between r and r + dr and with a size between R and R + dR.

Now, the L.H.S. of Equation (9) can be rewritten in an integral form using the above defined particle distribution function, Equation (19), as follows:

$$\int_{0}^{R_M} \int_{0}^{r_o} \frac{M(R)\,q(r)\,f(R)}{r}\,dr\,dR = \frac{1}{R_i}(\Gamma - M_i) + C_{eq} - C_b \quad \ldots (20)$$

Substitution of Equation (15) into Equation (2) and rewriting the size distribution function in a summation form yields:

$$\frac{3}{2}\left(\frac{4\pi}{3V_o}\right)^{1/3} \sum_{\ell=1}^{L} N_\ell M_\ell = \frac{1}{R_i}\left(\Gamma - M_i\right) + C_{eq} - C_b \qquad (21)$$

where, N_ℓ is number of particles within the ℓ-th group and L is the total number of groups of particles, each group defined by a certain size interval as in a histogram. Similar equations can be written for i = 1,2.....L, and the values of M_i are determined by solving L algebraic equations. The method by which Equations (2) and (21) are obtained is given in Appendix A.

When there is a non-uniform distribution, Equations (14) and (15) are not valid and Equation (21) is only approximate. An expression for q(r) and a modification of Equation (21) are described in Appendix B for non-uniform distributions.

The matrix composition is obtained by a mass balance between the particles and the matrix as follows:

$$-V_o \frac{dC_b}{dt} = \sum_{\ell=1}^{L} N_\ell \cdot 4\pi R_\ell^2 \left(C_p - C_\ell\right) \frac{dR_\ell}{dt} \quad . \tag{22}$$

Substitution of Equation (11) into Equation (22) yields:

$$\frac{dC_b}{dt} = \frac{4\pi D}{V_o} \sum_{\ell=i}^{L} M_\ell N_\ell \quad . \tag{23}$$

Finally, to completely describe the kinetics for an integrated time, we must account for the change in the size distribution function itself as some particles disappear and others either grow or shrink and enter a new size interval. According to Seybolt [18], this is done by using

$$\frac{\partial f(R)}{\partial t} = - \frac{\partial}{\partial R} \left[f(R) \frac{dR}{dt} \right] \tag{24}$$

In the results which follow, the above relationships are solved using a computer program based on the finite difference approximation of the derivatives. The method of calculation proceeds in the following sequence from time t to time, $t + \Delta t$.

1. calculation of L algebraic equations of Equation (21) to get values of M_i $(i = 1,2,\ldots,L)$;

2. calculation of Equation (11) to get dR_l/dt for $l = i - 1,2,\ldots,L$;

3. calculation of Equation (24) to obtain the size distribution at time $t + \Delta t$ based upon the values at time t; and

4. calculation of Equation (23) to obtain the matrix composition, C_b, at time $t + \Delta t$.

1. Application to Silica Particles in Copper

This system is suitable for the application of the model because the SiO_2 particles are spherical, and values of the physical properties such as interfacial energy and diffusivity are known. Furthermore, the SiO_2 particles are dispersed uniformly in internally oxidized copper [15].

Bhattacharyya and Russell [15] measured the change of the size distribution of silica particles in copper during isothermal homogenization. Some of their experimental results are shown as size distribution functions in Figures 1 - 3. Size distributions are obtained from their data by summing all of the particles with a radius R or less. This sum is $N(r_o,R)$ and since

$$N(r_o,R) = \int_o^R f(R)\,dR$$

then

$$f(R) = dN(r_o,R)/dR.$$

Thus from a plot of $N(r_o,R)$ versus R, f(R) is easily determined.

Bhattacharyya and Russell [15] used somewhat different experimental techniques in four series of homogenization treatments. The silica particles were obtained by internal oxidation of copper specimens containing silicon and then isolating them together with a copper-cuprous oxide mixture at the coarsening temperature. The temperature determined the partial pressure of oxygen, and hence the activity of oxygen in the copper-silica specimens. The silica particles from the coarsened samples were studied by electron microscopy using extraction replicas to measure the size distribution.

For calculations, the solubility product for SiO_2 in Cu is known only at 1000°C; it is [18]

$$C_{Si}\, C_O^2 = K, \quad K = 7.2 \times 10^{-11} \qquad (25)$$

Using the Van't Hoff equation and the heat of solution of SiO_2 in Cu, ΔH = 95 kcal/mole [19], we calculate the temperature dependency of the solubility as

$$K = 7.2 \times 10^{-11} \exp\left(37.6 - \frac{47,800}{T}\right) \qquad (26)$$

The coarsening kinetics are controlled by the diffusion of Si in Cu [15]. Then, considering the experimental conditions, we assume that the oxygen concentration in the copper matrix is the same as the solubility limit in the Cu-O binary system neglecting the effect of Si on the activity of oxygen; this is valid since the composition of silicon is less than 0.3%. The solubility of oxygen is given by:

$$C_O = 1.0952\left(\frac{T-273}{1,000}\right)^3 - 2.90215\left(\frac{T-273}{1,000}\right)^2 + 2.5640\left(\frac{T-273}{1,000}\right) - 0.7526$$

This relationship is from a regression analysis on data of the Cu-O binary system [20]. Other physical properties used in calculations are summarized in Table 1.

TABLE 1: Physical Properties Used for Calculations of Silica Coarsening in Copper

α	Interfacial energy, 2.39×10^{-5} cal/cm^2 [21]
V_m	Molar, volume, 27.3 cm^3/mole [22]
D	Diffusion coefficient, D = 0.037 exp(-40,000/R_g)cm^3/sec [23]

Calculated results are shown in Figure 1 to Figure 3 in the form of size distribution functions. In these calculations, we use the adjustable parameter, α, and modify the value of Γ in Equation (5) according to

$$\Gamma = \alpha \frac{2\sigma V_m C_{eq}}{R_g T} \tag{27}$$

Thus, if $\alpha = 1$ and the calculated curves agree with experiment, then the diffusion model predicts exactly the coarsening behavior of SiO_2 in copper. With $\alpha \neq 1$, the value selected is that which results in reasonable agreement between the calculations and experiments. As can be seen in Figures 1 - 3, the values of α differ and are not equal to unity so that there is not exact agreement between experimental results and calculations. The model predicts within a factor of ten which is as well as can be expected considering the many variables involved. Differences might be due to uncertainties of physical properties used in calculations such as interfacial energy or the solubility product for SiO_2. In particular, all the particles represented in Figures 1 - 3 are less than 1 micron radius and so there is probably a significant variation of interfacial surface energy with radius of curvature [9]. Other reasons might be that the extraction efficiency of the particles in the replica specimens was not 100 percent, or, as Battacharyya and Russell [15] concluded, the oxygen content in

the specimens did not equilibrate with the Cu-Cu_2O mixture in the expected manner.

To determine if particle coarsening is diffusion controlled, many workers reduce their data to the form of Equation (1), i.e., $\bar{R}^3$ vs. t. If a linear plot is obtained, then the kinetics are considered to be diffusion controlled. The experimental results of Bhattacharyya and Russell [15] and our calculated results are shown in Figure 4 in the form of Equation (1). Since we include a suitable value of α, as discussed above, experimental and calculated results compare well. However note that, in Figure 4c, the calculated curve is not linear which indicates that coarsening can be diffusion controlled, yet not obey Equation (1), the L.S.W. theory.

The major difference between the L.S.W. theory and our model is in the concentration profiles around the particles. In the L.S.W. theory, the concentration profile is given by the steady state distribution around isolated spheres with the diffusion potential given by the difference in matrix composition at the matrix-particle interface and in the "bulk" matrix; that formulation, therefore, neglects the direct effect of surrounding particles. In our model, which is a modification of the model given by Weins and Cahn [11,12], the effect of surrounding particles is incorporated because

the system of particles is comprised of system of point potentials given by the respective radii of curvature of the individual particles and no assumption is made regarding the concentration profile around the individual particles.

2. Application of the Model to MnS Inclusions in Low Alloy Steel

The model is applied to the experimental results of one of the authors [16,17] on the coarsening of sulfides in AISI 4340 low alloy steel during homogenization treatment. Specimens were removed from a cast ingot and homogenized in a vacuum furnace at 1315°C for times between 20 and 100 hours. The specimens were metallographically prepared and examined unetched using light microscopy. Results were reduced into suitable form by applying quantitative metallographic techniques.

Figure 5 shows the measured size distributions after homogenization treatments of various durations. In the model calculations, sulfide inclusions are assumed to be pure MnS due to the high composition of manganese (Table 2). Another assumption is that the rate controlling step is the diffusion of sulfur in the matrix because of the low solubility of sulfur in austenite.

TABLE 2: Composition of AISI 4340 Ingot in Weight Percent [17]

C	Si	Mn	P	S	Al	Ni	Cr	Mo
0.46	0.26	0.61	0.007	0.017	0.04	1.75	0.88	0.16

The solubility product for MnS used in calculations is from Turkdogan et al [24]:

$$\log f_s = -\frac{215}{T} + 0.097\, C_{Mn} \quad (28)$$

$$C_{Mn} \cdot C_S f_s = K \quad (29)$$

$$\log K = -\frac{9020}{T} + 2.929 \quad (30)$$

where C_{Mn} and C_S are the compositions of manganese and sulfur, respectively, in weight percent and f_s is the activity coefficient of sulfur. The effect of other alloying elements on the solubility limit are neglected, because carbon [25] and silicon [26] do not have much effect, and there are no data available for the other elements, such as Ni, Cr and Mo. Physical properties used in calculations are shown in Table 3.

Figures 6 and 7 show the comparison of calculated results with experimental results. In these calculations, the

TABLE 3: Physical Properties Used for Calculation of Coarsening of Manganese Sulfide Inclusions in AISI 4340 Low Alloy Steel

σ	Interfacial energy, 1.2×10^{-5} cal/cm^2 [16]
V_m	Molar volume, 21.8 cm^3/mole [27]
D	Diffusion coefficient, $D = 1.7 \exp(-53{,}000/R_g)$ cm^2/sec [23]

parameter α is 1, which means no modification of physical properties. In Figure 6, the comparisons are shown in the form of the size distribution function, rather than a histogram, for the sake of convenience. Figure 7 shows the comparison between calculations and experiments on the time change of average radius, $\bar{R}$, volume percent, V, total number, N, and interfacial areas, S, of sulfide inclusions during homogenization treatment. Both figures indicate that there is excellent agreement between calculated and experimental results even without α deviating from unity. That there is such an excellent comparison between calculated results and experiment might not be entirely fortuitous in this case because the particles are, for the most part, greater than 1 micron in diameter, and so the size effect on interfacial energy is probably not significant. In addition, one need not consider

error due to extraction efficiencies since light microscopy was employed to obtain the experimental results.

Notice in Figure 8 that the model and experimental results do not predict a linear relationship between the cube of the average radius, $\bar{R}^3$, and time as is predicted by the often-used L.S.W. theory, Equation (1).

3. Predicted Behavior of Manganese Sulfide Inclusions

Since the model compares well with the coarsening of manganese sulfide inclusions during high temperature treatment, we have used the model to predict the behavior of manganese sulfide inclusions in steels of various manganese content, ranging from 0.1 to 1.2%, and with a "high" level of sulfur (0.017%), as well as for a "low" sulfur steel (0.003%).

Figure 9 shows the effects of manganese concentration on the coarsening for 0.017% S. Generally, all sulfides formed are pure MnS at the manganese compositions above 0.3% [24] but below this level, the sulfides probably contain some iron. Therefore, our assumption of pure MnS is valid above 0.3% manganese concentration range, and below this concentration, such as 0.1% Mn, calculated results of the matrix-composition are in error. As expected from the thermodynamic data,

manganese has a significant effect on the coarsening through its strong effect on the solubility limit of sulfur. For these calculations, the initial size distribution in Figure 9a is that shown in Figure 6 as the initial condition.

Figure 10 shows the effects of manganese on the average radius, $\bar{R}$, and the total number of sulfide inclusions, N, for high and low sulfur steels. For the initial size distribution of low sulfur steel, we modified the initial size distribution of high sulfur steel obtained experimentally (Figure 6) by decreasing the number of sulfide inclusions in proportion to the ratio of sulfur between the two cases, i.e., 0.003:0.017.

Our calculations indicate very little difference between the average radius of low and high sulfur steel so the results are presented in one graph. These results show that manganese decreases the rate of coarsening, and this effect is dominant throughout the homogenization period.

Figure 11 shows the relationship between manganese composition and relative number (number of particles/initial number) of sulfide inclusions for 10 and 100 hours homogenization. The difference between low and high sulfur is negligible and the effect of manganese concentration is more dominant for 10 hours, and somewhat less after 100 hours. For 100 hours

homogenization, an increase in manganese above 0.6% does not have a significant effect on the coarsening kinetics. Figure 11 also indicates the difficulty of dissolving MnS inclusions even when the steel is heated to a temperature greater than the austenite-MnS solvus. For example, at 1315°C, the solubility of sulfur in austenite for 0.3% Mn is 0.007% S. Yet, after 10 hours at 1315°C, 55 percent in number of the original manganese sulfide inclusions remain (Figure 11) in steel containing 0.003% S, and after 100 hours, there still remains 30 percent.

Figures 12 and 13 show the effects of the homogenization temperature on the coarsening of the manganese sulfide inclusions. As expected from the temperature dependence of diffusivity and solubility limit of sulfur, temperature has a significant effect on the coarsening kinetics. At a high temperature, the coarsening proceeds rapidly for the early stage of homogenization and, after that, the rate slowly decreases. On the other hand, at a low temperature, the coarsening proceeds constantly throughout homogenization time and in terms of average radius is almost linear with time. Obviously, Equation (1) cannot be applied to these results, as is also the case with SiO_2 particles in copper for the reasons previously discussed.

Figure 13 shows the effects of the homogenization temperature on the average radius and relative number of sulfide inclusions after 10 and 100 hours, for low and high sulfur steels; there is no significant difference between the low and high sulfur steels. After 10 hours, the coarsening has proceeded rapidly above 1250°C, and no significant coarsening has occurred below 1200°C. On the other hand at 100 hours, significant coarsening occurs for temperatures as low as 1100°C.

IV. CONCLUSIONS

A model to simulate the coarsening and dissolution kinetics of second phase particles within a metallic matrix was formulated. Application of this model to the coarsening kinetics of SiO_2 particles in a copper matrix revealed that the model predicts the change in size distributions (provided that the parameter α is adjusted) during isothermal high temperature treatment. To describe the kinetics of the morphological changes of sulfide inclusions in steel, no adjustments in the model were necessary, and excellent agreement was obtained between calculations and experiments.

Some calculations were carried out to predict the behavior of sulfide inclusions during high temperature treatments (as in homogenization and soaking for hot working) and the following results were obtained.

1. The composition of manganese has a significant effect on the coarsening kinetics of manganese sulfide inclusions in steel; the rate of coarsening is decreased by increasing manganese concentration.

2. The effect of manganese is more dominant in short-time homogenization (10 hours) than in long-time (100 hours) homogenization at 1315°C. Above 0.6% Mn, an increase in

manganese does not have a significant effect on the coarsening kinetics for 100 hours homogenization.

3. Temperature significantly affects the kinetics. After 10 hours homogenization, no effective change is observed in the size distribution below 1200°C, but at 100 hours, the extent of coarsening (expressed as average radius) increases linearly with increasing temperature in the range of 1100 to 1400°C.

4. Sulfur concentration does not influence the rate of change of average radius and only slightly influences the decrease in the relative number of inclusions (number of inclusions/original number of inclusions) during homogenization, assuming that the number of sulfides before homogenization is proportional to the composition of sulfur.

5. According to calculations, the rate of dissolution of manganese sulfide inclusions is very slow, even when the temperature is in excess of the austenite-sulfide solvus temperature.

Our calculations also indicate that the coarsening kinetics of second phase particles are not adequately described by the often-used relationship (i.e., Equation (1))

which predicts that the cube of the average radius of particles increases linearly with time.

ACKNOWLEDGEMENTS

The work reported here was conducted under the sponsorship of Army Materials and Mechanics Research Center, Watertown, Ma. One of the authors (T. Fujii) would like to thank the Kawasaki Steel Corporation, Japan, for the opportunity to carry out the research at MIT.

APPENDIX A

Derivation of Equations (20) and (21)

According to Equation (9) it is necessary to assume the ratio of pole strength to radius for all particles in the system. First we define M(R) as the pole strength of a particle with radius R and N_R as the number of particles with a radius from R to R + ΔR. Then

$$\sum_{j=1}^{N_R} \frac{M_j}{r_{ij}} = \sum_{k=1}^{K} \frac{M(R)f(R)q(r_k)\Delta r \Delta R}{r_k} \qquad (A1)$$

where K is the number of intervals by which distance is subdivided uniformly, i.e.,

$$K = \frac{r_o}{\Delta r} ,$$

and k is the number of a specific interval, i.e.,

$$k = \frac{r_k}{\Delta r} .$$

With a large number of intervals, $K \to \infty$ and $\Delta r \to 0$, then

$$\sum_{j=1}^{N_R} \frac{M_j}{r_{ij}} = \int_{o}^{r_o} \frac{M(R)f(R)\Delta R\, q(r)}{r}\, dr \qquad (A2)$$

AD-A097 469 MASSACHUSETTS INST OF TECH CAMBRIDGE DEPT OF MATERIA--ETC F/G 11/6
SULFIDE INCLUSIONS IN ELECTROSLAG REMELTED STEELS.(U)
JAN 81 M D BOLDY, T FUJII, D R POIRIER DAAG46-78-C-0032
UNCLASSIFIED AMMRC-TR-81-4 NL

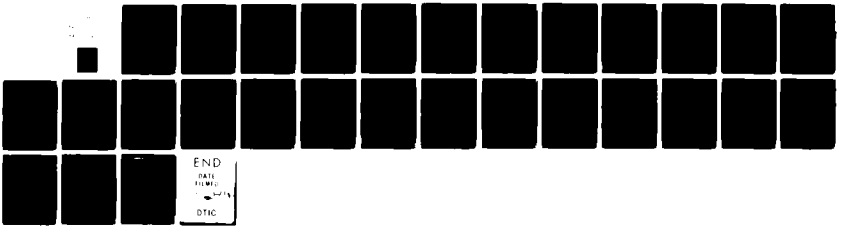

END
DATE FILMED
DTIC

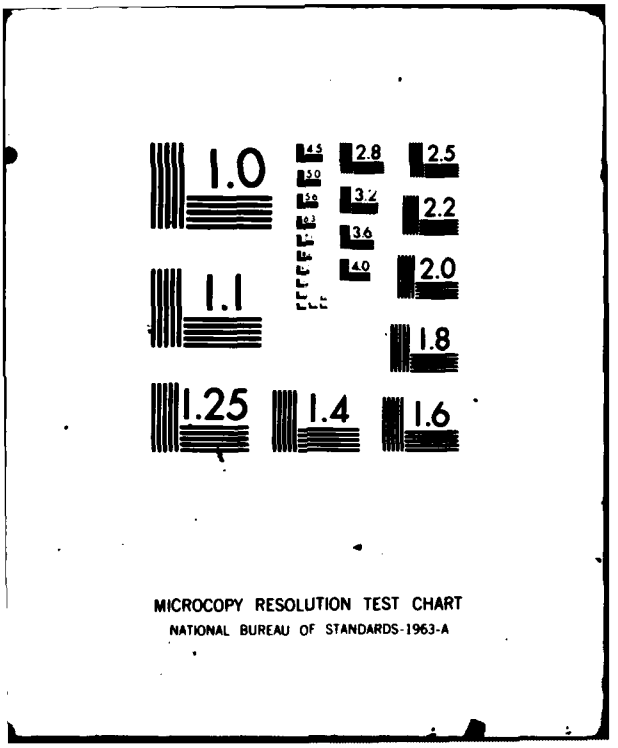
1.0
1.1
1.25
1.4
1.6
2.8
2.5
3.2
2.2
3.6
2.0
4.0
1.8
MICROCOPY RESOLUTION TEST CHART
NATIONAL BUREAU OF STANDARDS-1963-A

Now consider all particles, N, with radius from zero to R_M (the largest particles), then

$$\sum_{j=1}^{N} \frac{M_j}{r_{ij}} = \int_o^{r_o} \frac{q(r)}{r}\, dr \cdot \sum_{\ell=1}^{L} M(R_\ell) f(R_\ell) \Delta R \qquad (A3)$$

where L is the number of groups of particles by which the total number is subdivided, according to size, i.e.,

$$L = \frac{R_M}{\Delta R} ,$$

and ℓ is the number of the size group. If $L \to \infty$, then

$$\sum_{j=1}^{N} \frac{M_j}{r_{ij}} = \int_o^{R_M} \int_o^{r_o} \frac{M(R) f(R) q(r)}{r}\, dr dR \qquad (A4)$$

Equations (9) and (A4) are combined to obtain Equation (20). When the particles are uniformly distributed, Equation (15) applies and

$$\int_o^{R_M} \int_o^{r_o} \frac{M(R) f(R) q(r)}{r}\, dr dR =$$

$$\int_o^{R_M} M(R) f(R)\, dR \int_o^{r_o} \frac{q(r)}{r}\, dr =$$

$$\frac{3}{2} \left(\frac{4\pi}{3V_o}\right)^{1/3} \int_o^{R_M} M(R) f(R)\, dR \; . \qquad (A5)$$

If we wish to subdivide our particles according to sizes as in a histogram, then it is more convenient to express the integral of the R.H.S. of Equation (A5) as a summation. This is

$$\int_{0}^{R_M} M(R) f(R) dR = \sum_{\ell=1}^{L} N_\ell M_\ell \qquad (A6)$$

where N_ℓ is the number of particles within the ℓ-th group and M_ℓ is the pole strength of particles with radius $R + 1/2\ \Delta R$ within the group. By combining Equations (A5), (A6) and (20), one obtains Equation (21).

APPENDIX B

Non-uniform Particle Distribution

With a non-uniform distribution, an approach to describe the distribution of particles is to select a reference region, as illustrated in Figure 14. In the regions where the particles are clustered or dispersed

$$q(r) \propto r^{2\gamma} \qquad (B1)$$

where $\gamma \neq 1$. Substitution of Equation (B1) into Equations (12) and (13) yields:

$$q(r) = \left(2\gamma + 1\right)\left(\frac{4\pi}{3V_o}\right)^{(2\gamma+1)/3} r^{2\gamma} \qquad (B2)$$

where, $\gamma > 1$ non-uniform (dispersed),

$\gamma < 1$ non-uniform (clustered), and

$\gamma = 1$ uniform.

When $\gamma = 1$, Equation (B2) reduces to Equation (15).

With Equation (B2), we can obtain a more general form of Equation (21) for non-uniform distribution of particles in the matrix:

$$\left(\frac{2\gamma+1}{2\gamma}\right)\left(\frac{4\pi}{3V_o}\right)^{1/3} \sum_{\ell=1}^{L} N_\ell M_\ell = \frac{1}{R_i}\left(\Gamma - M_i\right) + C_{eq} - C_b \qquad (B3)$$

Figure 15 shows examples of q(r) versus distance from a reference particle.

LIST OF SYMBOLS

A	area for diffusion, Equation (2)
C	solute concentration
C_b	solute concentration in bulk matrix
C_{eq}	equilibrium concentration (i.e., matrix solubility)
C_p	solute concentration in particle
D	diffusivity
$f(R)$	size distribution function
K	number of groups of particles subdivided according to distance r
L	number of groups of particles subdivided according to size range
M	constant introduced in Equation (6); sometimes called "pole strength"
N	number of particles or inclusions
n_g	number of groups of particles, each group of certain size interval
N_o	number of particles before homogenization
$q(r)$	space distribution function of particles
R	radius of particle or inclusion
$\bar{R}$	average radius of particles or inclusions
R_g	gas constant
$\bar{R}_o$	average radius at time zero
R_M	maximum radius of particles or inclusions
r	distance from a point in space
$\underset{\sim}{r}$	vector in space

S surface area of particle

T absolute temperature

t time

V_m molar volume

V_o volume of sphere with radius r_o; i.e., size of sample

x effective diffusion length in Equation (2)

x_L average interparticle spacing

α particle-matrix interfacial energy

ρ mass density of particle

Γ $2\sigma C_{eq}/R_g T$

Subscripts

i,j are for individual particles

k,ℓ are for groups of particles

REFERENCES

1. R. A. Tanzilli and R. W. Heckel, Trans. TMS-AIME, 1968, vol. 242, p. 2313.

2. M. J. Whelan, Met. Sci. J., 1969, vol. 3, p. 95.

3. H. B. Aaron, D. Fainstein and G. R. Kotler, J. Appl. Phys., 1970, vol. 41, p. 4404.

4. B. Karlsson and L. E. Larsson, Mat. Sci. and Eng., 1975, vol. 20, p. 161.

5. T. M. Ahn and J. K. Tien, J. Phys. Chem. Solids, 1976, vol. 37, p. 771.

6. S. K. Bhattacharya and K. C. Russell, Met. Trans., 1972, vol. 3, p. 2195.

7. C. Wagner, Zeit. fur Electrochemie, 1961, vol. 65, p. 581.

8. I. M. Lifshitz and V. Slyozov, J. Phys. Chem. Solids, 1961, vol. 19, p. 35.

9. G. W. Greenwood, Acta Met., 1956, vol. 4, p. 243.

10. R. W. Heckel, Trans. TMS-AIME, 1965, vol. 233, p. 1994.

11. J. J. Weins, Ph.D. Thesis, Dept. Mat. Sci. and Eng., M.I.T., Cambridge, Mass., 1970.

12. J. J. Weins and J. W. Cahn, Materials Science Research, Sintering and Related Phenomena, vol. VI, 1973, pp. 151-163.

13. G. R. Speich and R. A. Oriani, Trans. TMS-AIME, 1965, vol. 233, p. 623.

14. J. D. Livingston, Trans. TMS-AIME, 1959, vol. 215, p. 566.

15. S. K. Bhattacharyya and K. C. Russell, Met. Trans., 1976, vol. 7A, p. 453.

16. D. Gnanamuthu, T. Z. Kattamis, M. C. Flemings and R. Mehrabian, Met. Trans., 1974, vol. 5, p. 2557.

17. D. Gnanamuthu, M. Basaran, T. Z. Kattamis, R. Mehrabian and M. C. Flemings, U.S. Army Materials and Mechanics Research Center, Watertown, Ma., Contract No. DAAG46-68-C-0043, 1971.

18. A. Y. Seybolt, Oxide Dispersion Strengthening, Met. Soc. Conference, vol. 47, 1966, p. 469.

19. S. K. Bhattacharyya, Ph.D. Thesis, Dept. Mat. Sci. and Eng., M.I.T., Cambridge, Ma., 1972.

20. A. Phillips and E. N. Skinner, Trans. TMS-AIME, 1941, vol. 143, p. 301.

21. L. H. Van Vlack, Elements of Materials Science, 2nd ed., Addison-Wesley, Ma., 1953, p. 349.

22. F. N. Rhines and R. F. Mehl, Trans. AIME, 1938, vol. 128, p. 185.

23. A. Hoshino and T. Araki, Tetsu to Hagane, 1970, vol. 56, p. 252.

24. E. T. Turkdogah, S. Ignatowicz and J. Pearson, J.I.S.I., 1955, vol. 180, p. 349.

25. A. M. Barloga, K. R. Bock and N. Parlee, Trans. TMS-AIME, 1961, vol. 221, p. 173.

26. H. C. Fiedler, Trans. TMS-AIME, 1967, vol. 239, p. 260.

27. R. C. Weast (ed.), Handbook of Chemistry and Physics, 57th Edition, CRC Press, Cleveland, Ohio, 1976.

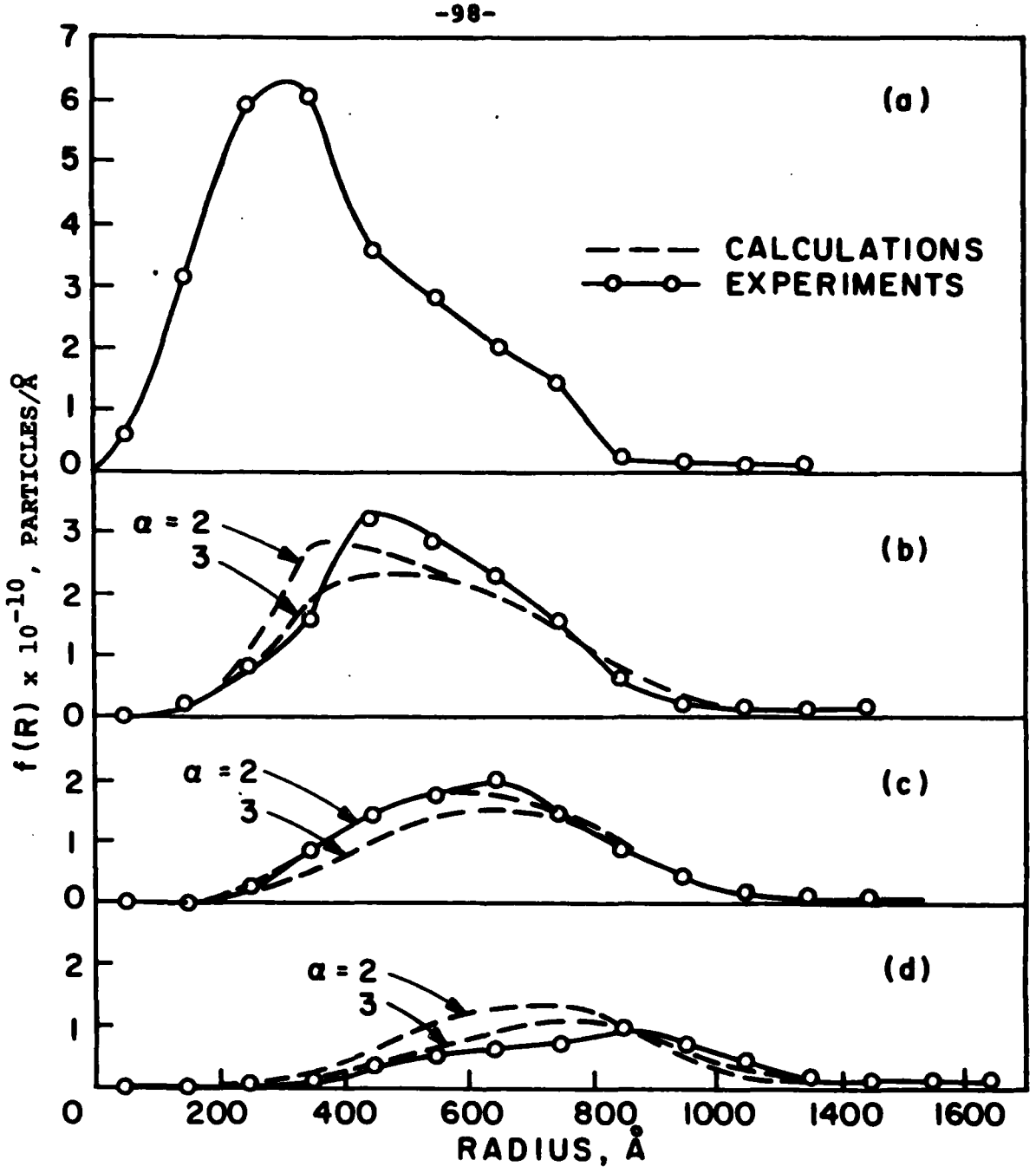

Figure 1 Comparisons of calculated size distributions and experimental results of silica coarsening in copper at 1000°C for (a) 8 h, (b) 27 h, (c) 64 h, and (d) 125 h. Experiments are series 1 - 1 from Reference 15.

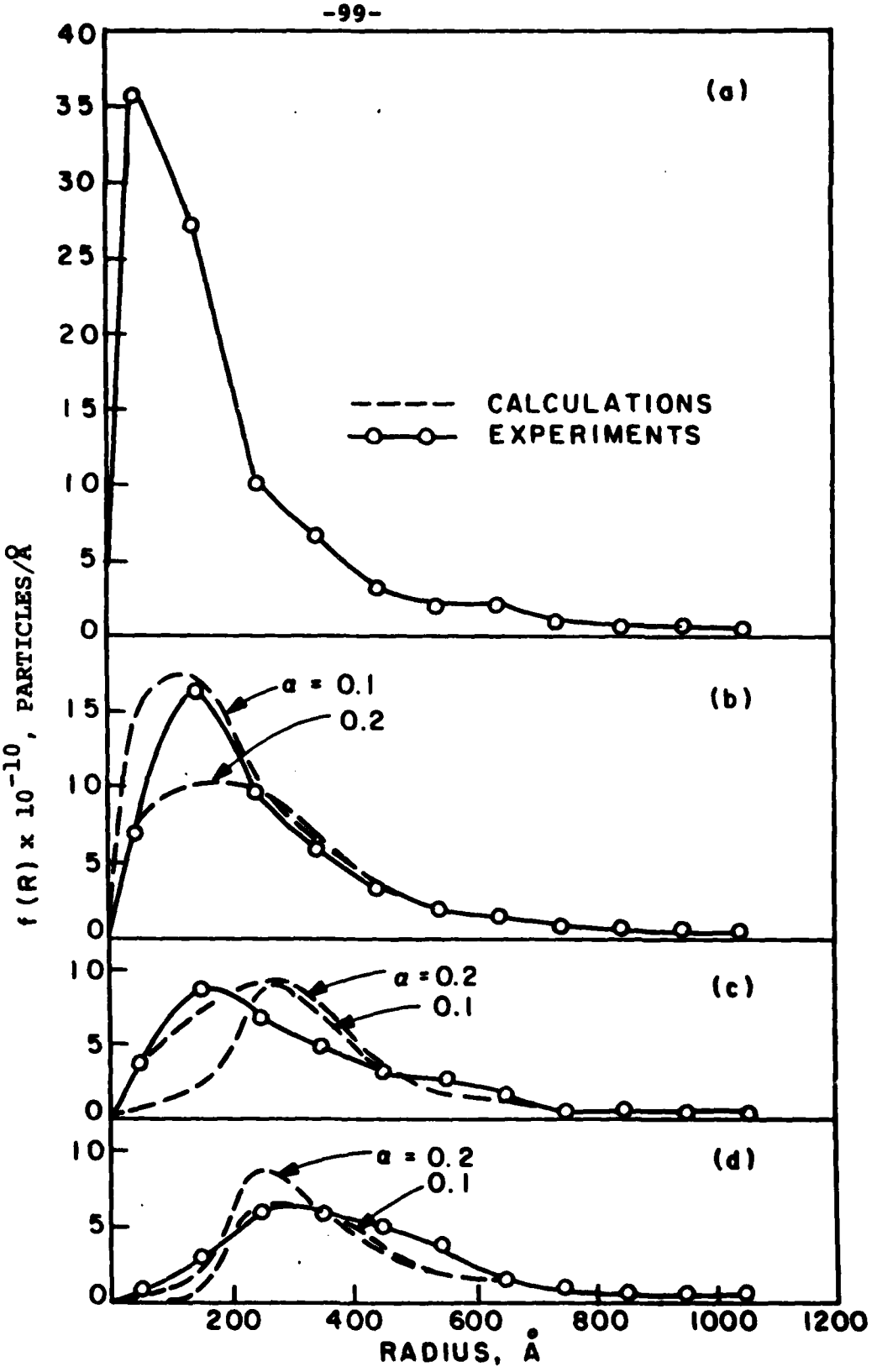

Figure 2 Comparisons of calculated size distributions and experimental results of silica coarsening in copper at 950°C for (a) 8 h, (b) 27 h, (c) 64 h, and (d) 140 h. Experiments are series 1 - 2 from Reference 15.

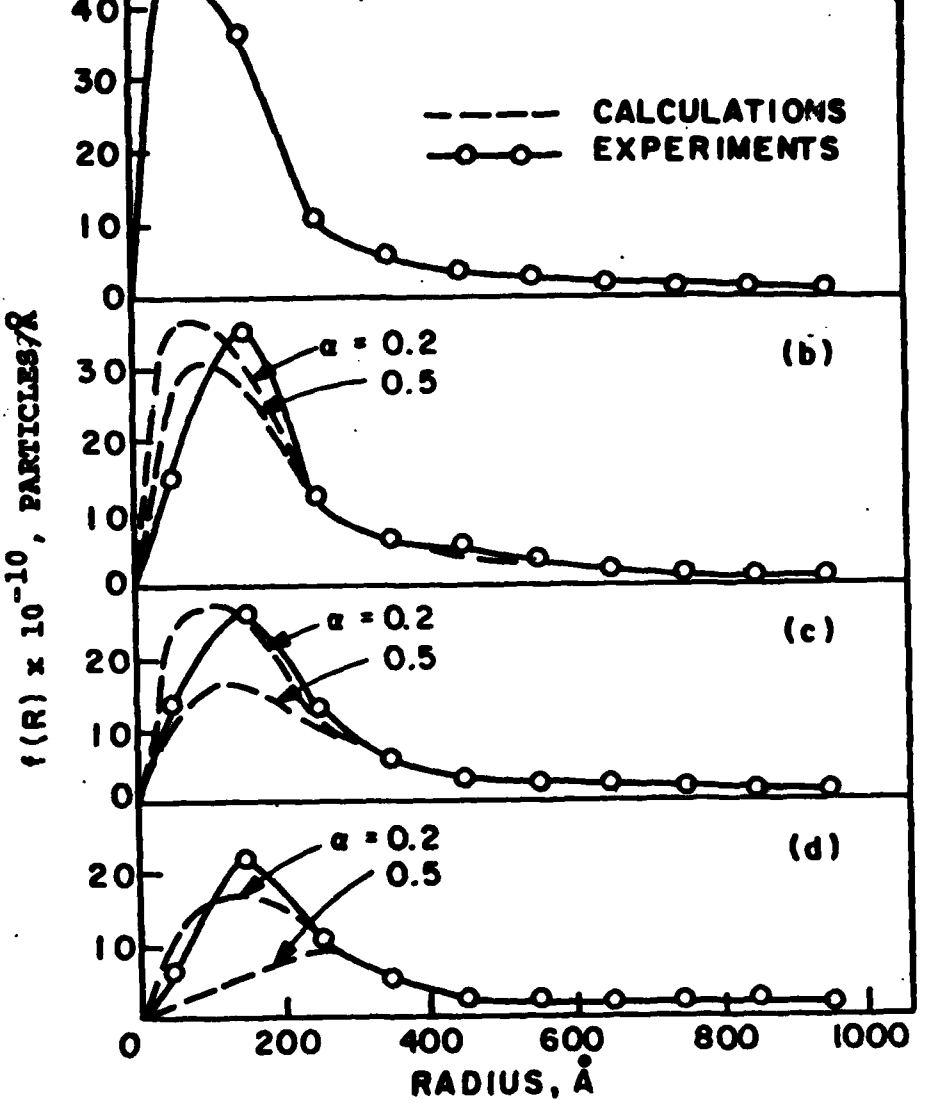

Figure 3 Comparisons of calculated size distributions and experimental results of silica coarsening in copper at 900°C for (a) 8 h, (b) 27 h, (c) 64 h and (d) 140 h. Experiments are series 1 - 3 from Reference 15.

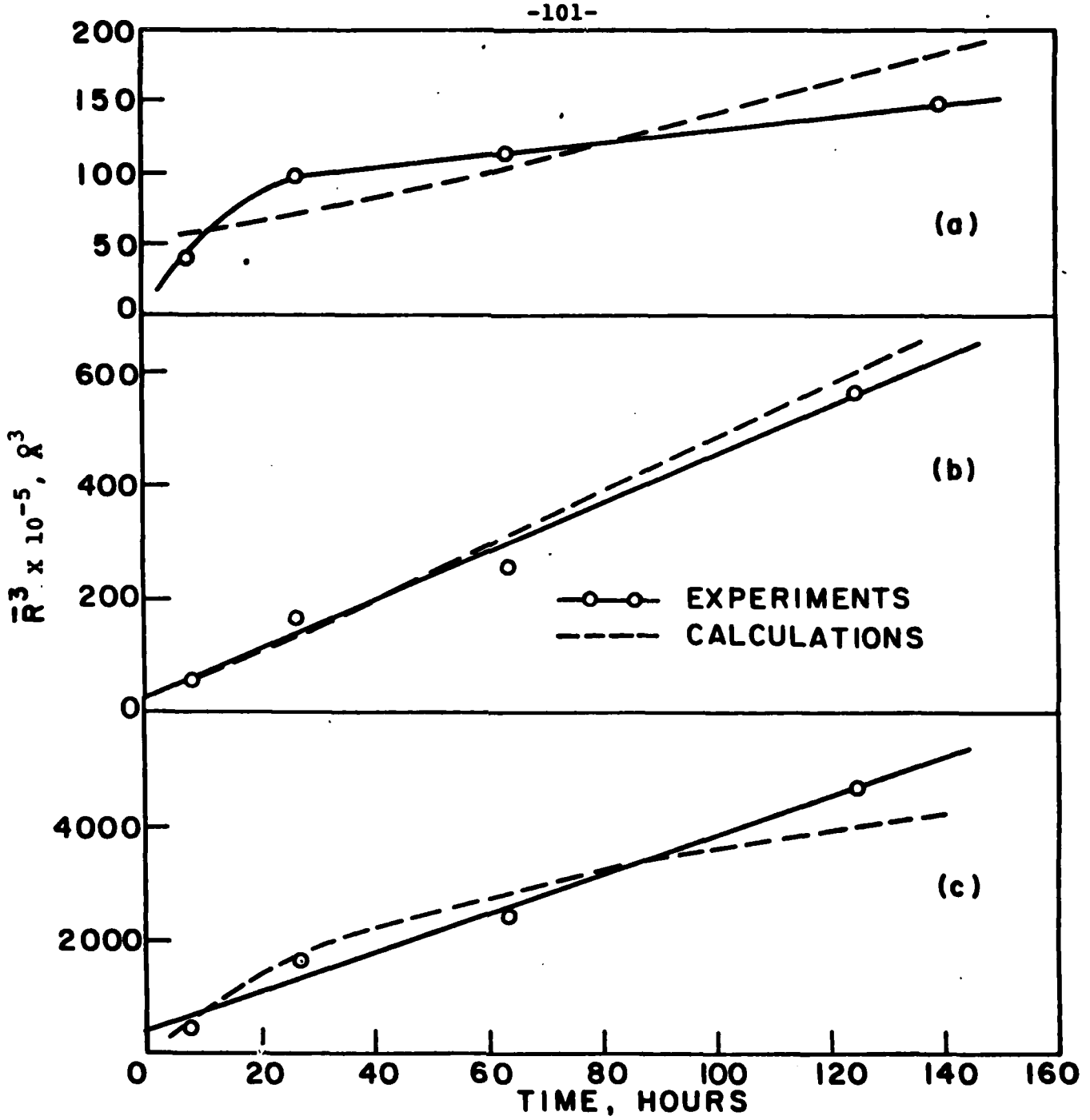

Figure 4 Comparison of calculations and experiments for the coarsening of silica in copper in terms of average radius versus time. Coarsening temperatures and values of α are (a) 900°C, $\alpha = 0.2$, (b) 950°C, $\alpha = 0.1$, and (c) 1000°C, $\alpha = 3$. Experimental results are from Reference 15.

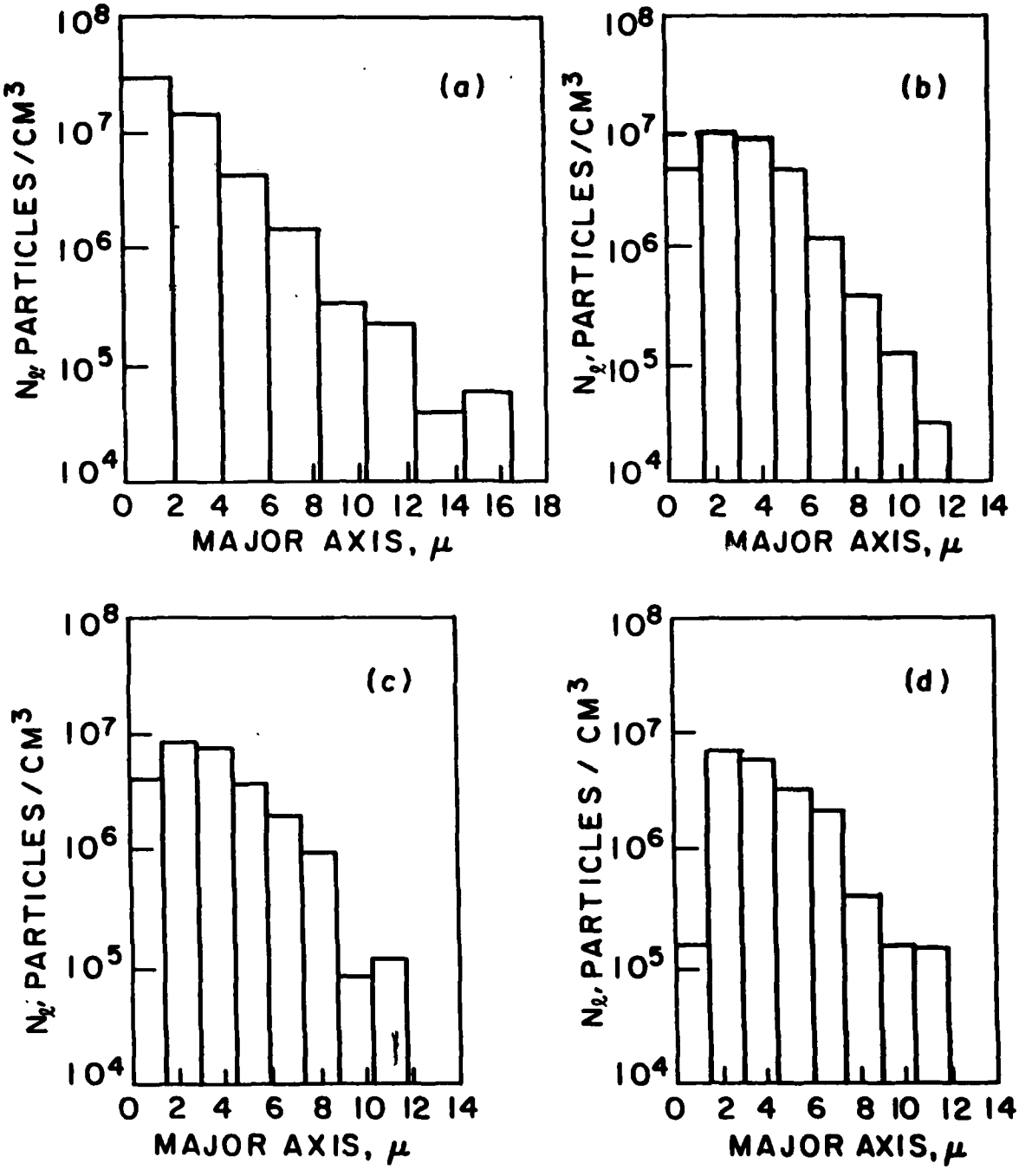

Figure 5 Size distributions of manganese sulfide inclusions in AISI 4340 low alloy steel: (a) as-cast. Homogenized at 1315°C: (b) 21 h, (c) 49 h, and (d) 100 h. From Reference 16.

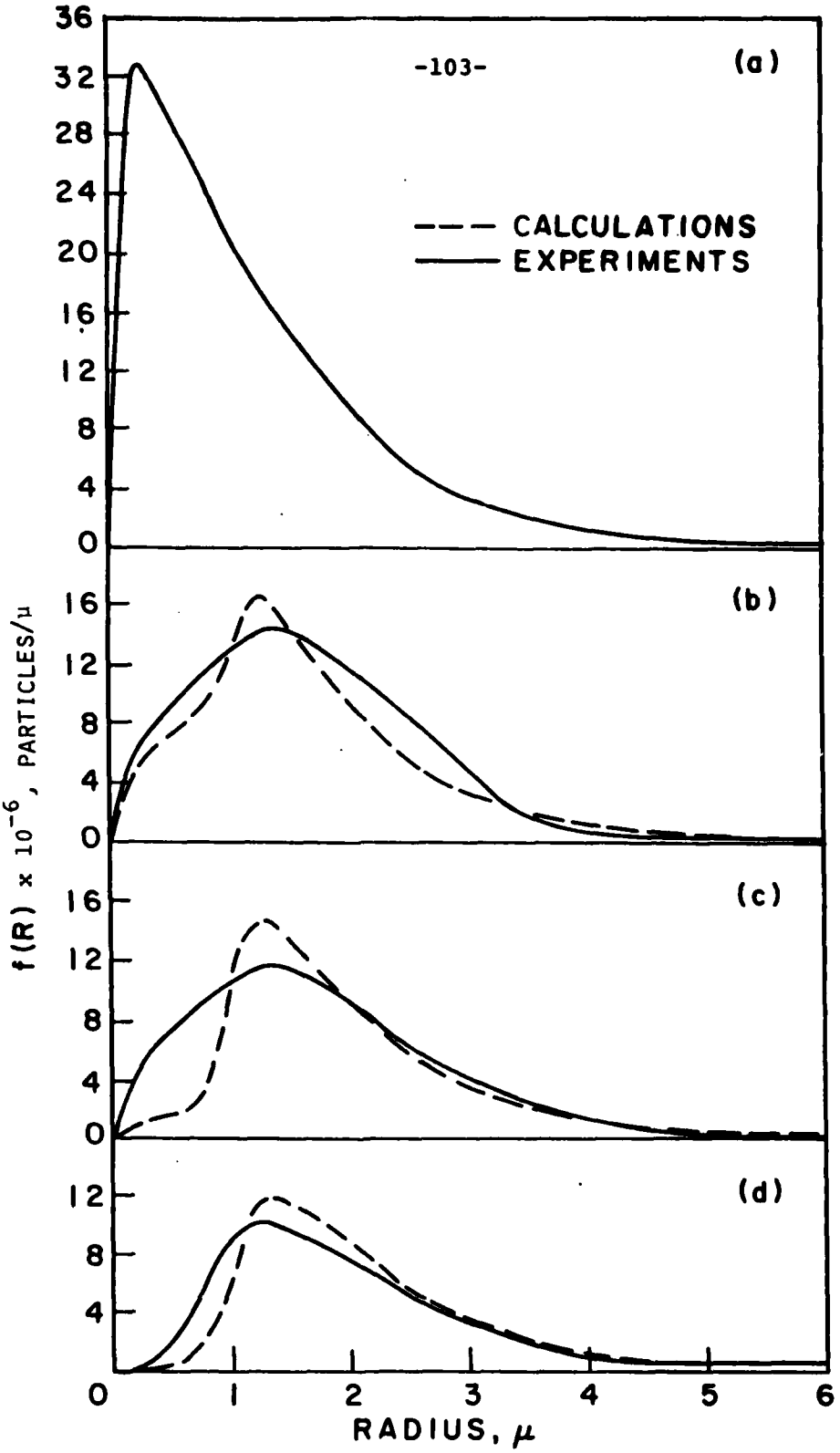

Figure 6 Comparison of calculations and experiments for the coarsening of manganese sulfide inclusions in 4340 low alloy steel at 1315°C. (a) As-cast and initial distribution, (b) 21 h, (c) 49h, and (d) 100 h. Experimental results are from Reference 16.

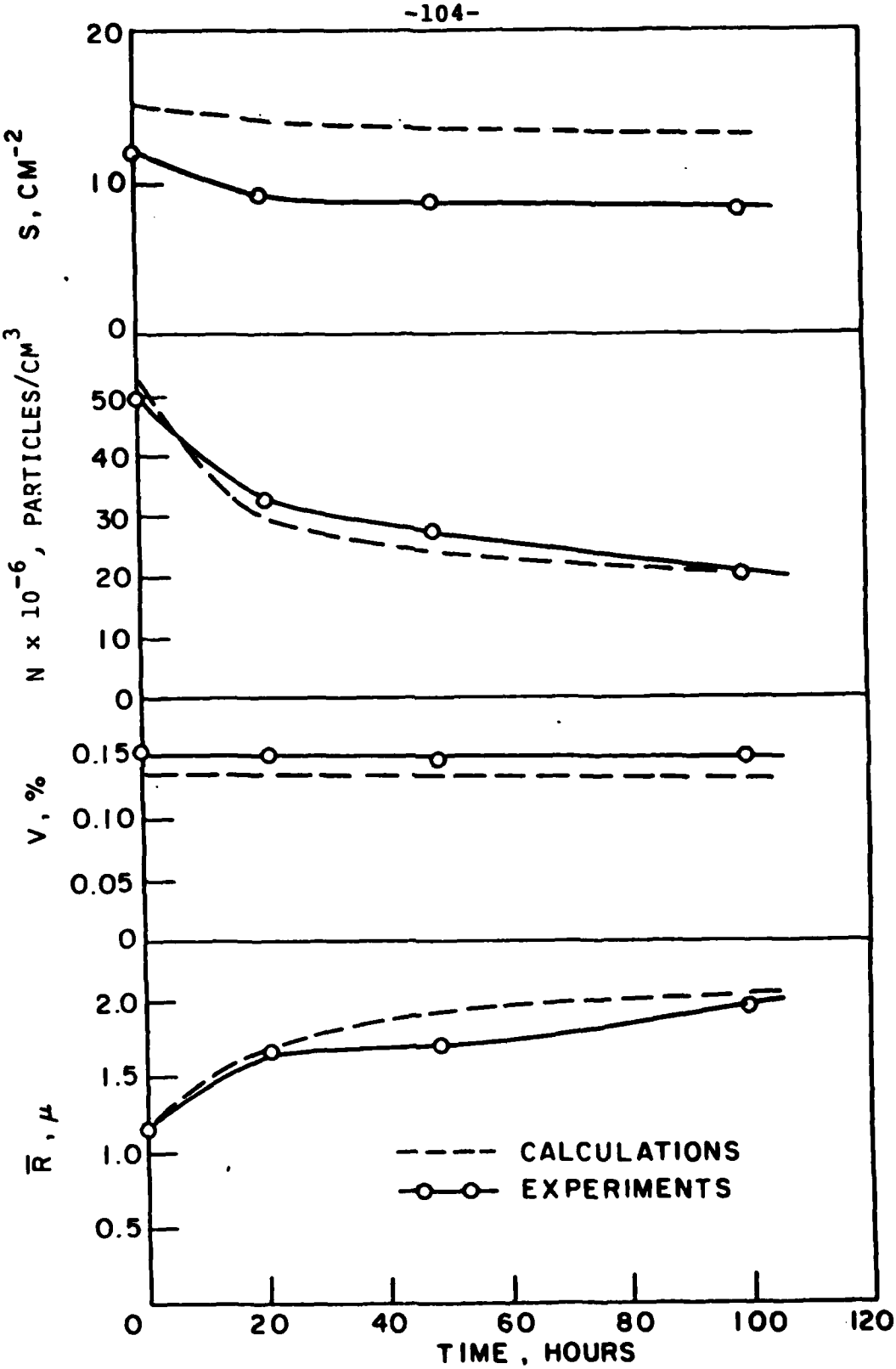

Figure 7 Comparison of calculations and experiments on average radius, $\bar{R}$, volume percent, V, total number, N, and surface area, S, of manganese sulfide inclusions in 4340 low alloy steel homogenized at 1315°C. Experimental results are from Reference 16.

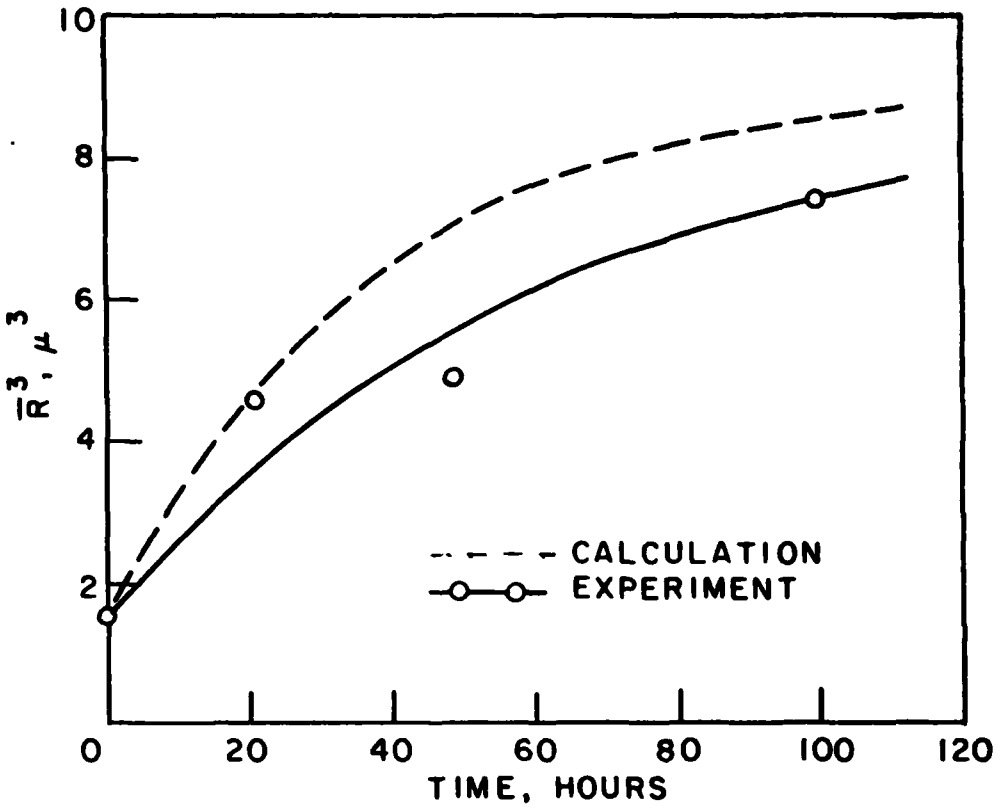

Figure 8 Comparison of calculations and experiments on the homogenization time versus cube of average radius, for 4340 low alloy steel homogenized at 1315°C. Experimental results are from Reference 16.

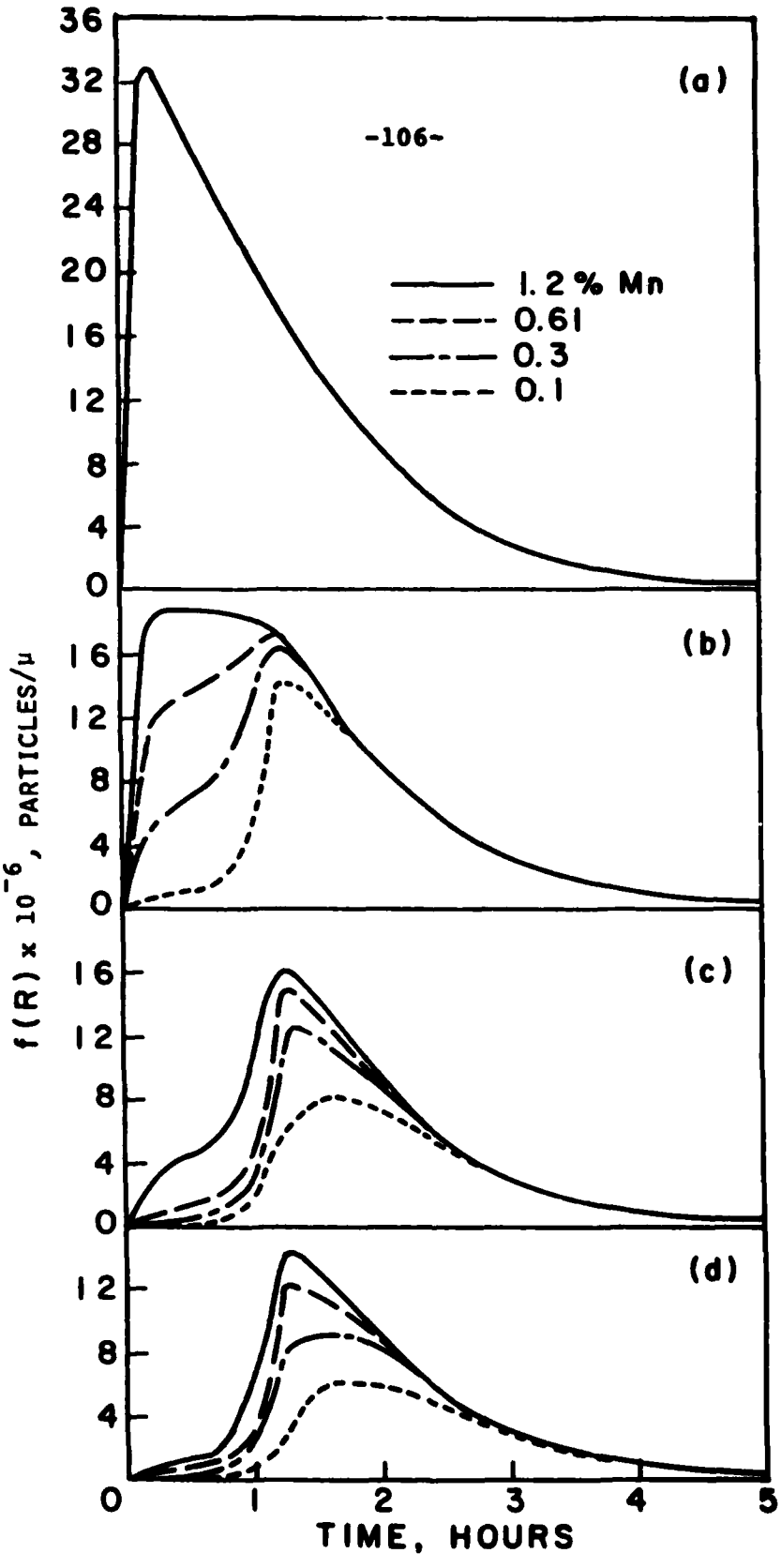

Figure 9 The effect of manganese concentration on the size distribution of manganese sulfide inclusions in steel. Calculations are for homogenization at 1315° for times of (a) 0 h (initial distribution), (b) 10 h, (c) 50 h and (d) 100 h.

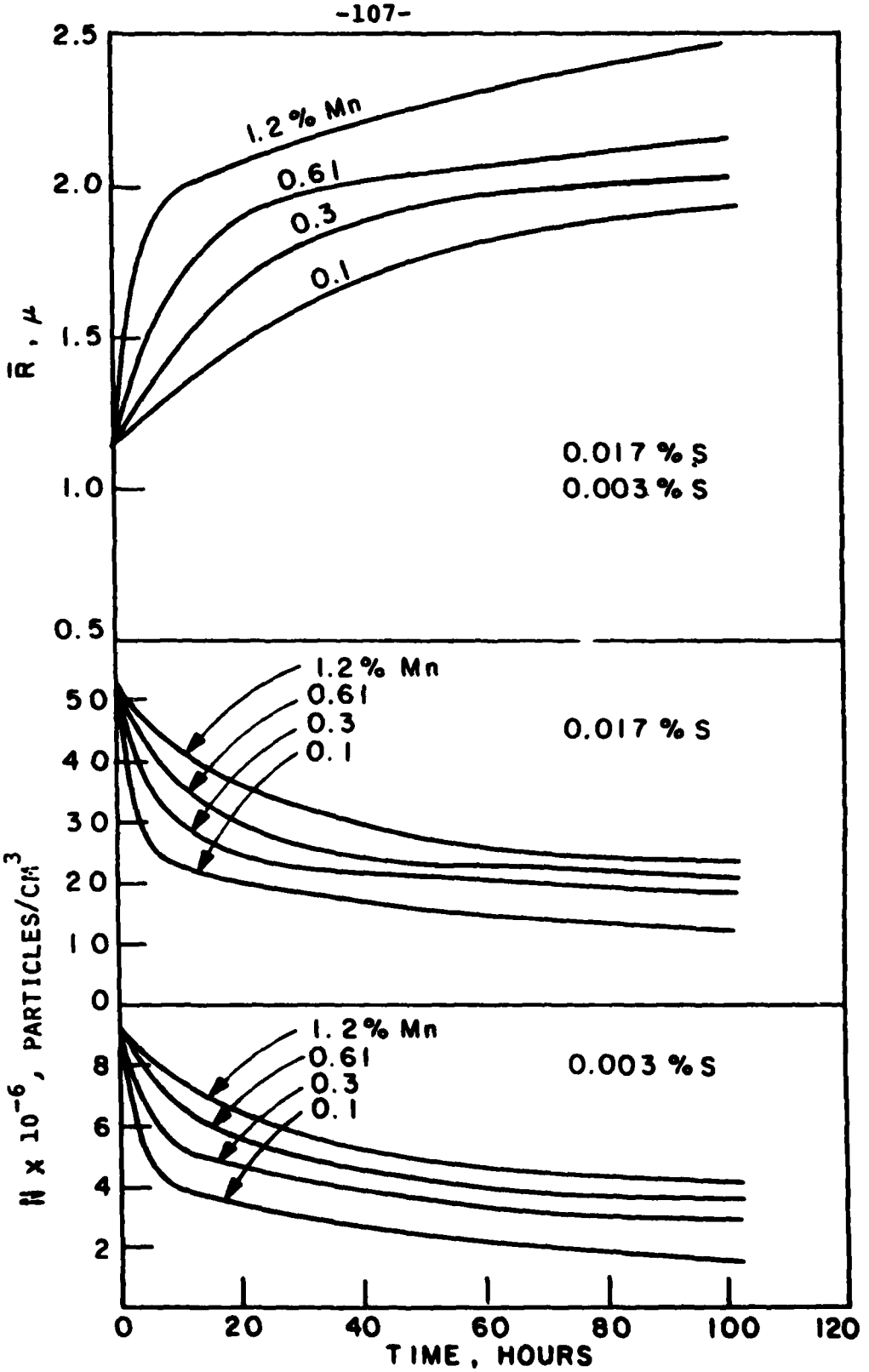

Figure 10 The effect of manganese concentration on the coarsening of manganese sulfide inclusions in steel. Calculations are for average radius, $\bar{R}$, and number of particles, N.

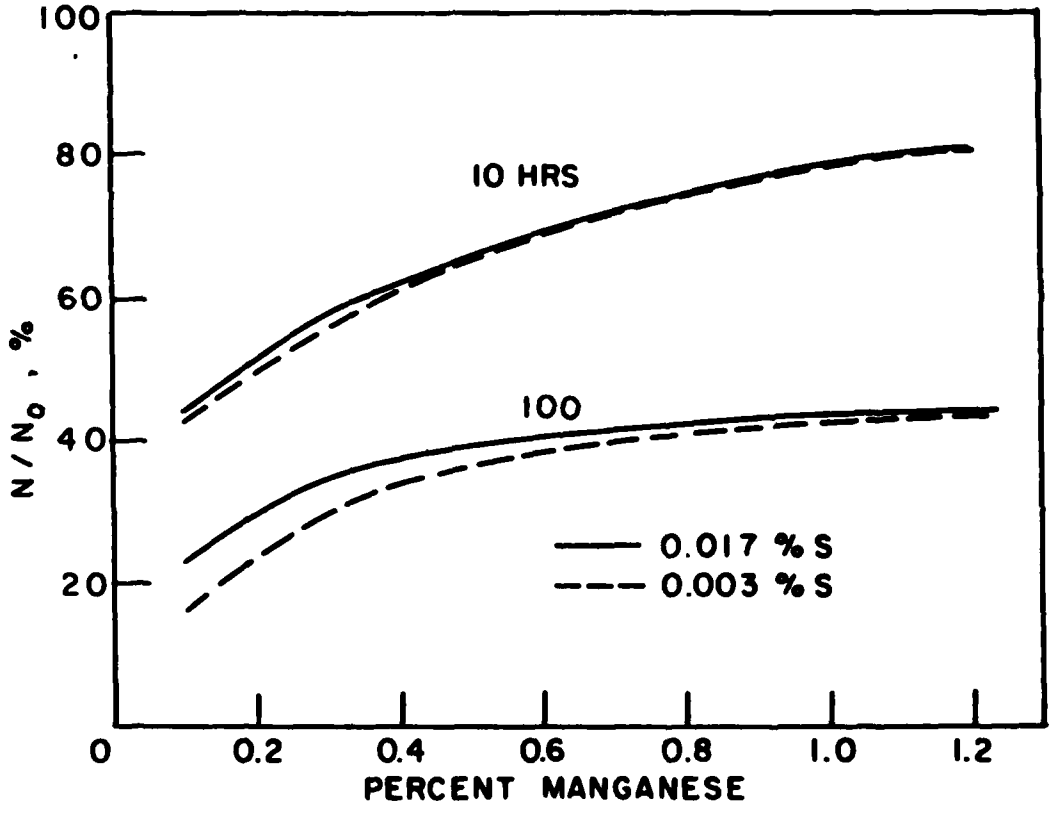

Figure 11 The relative number of undissolved manganese sulfide inclusions as calculated for various manganese concentrations in steel at 1315°C.

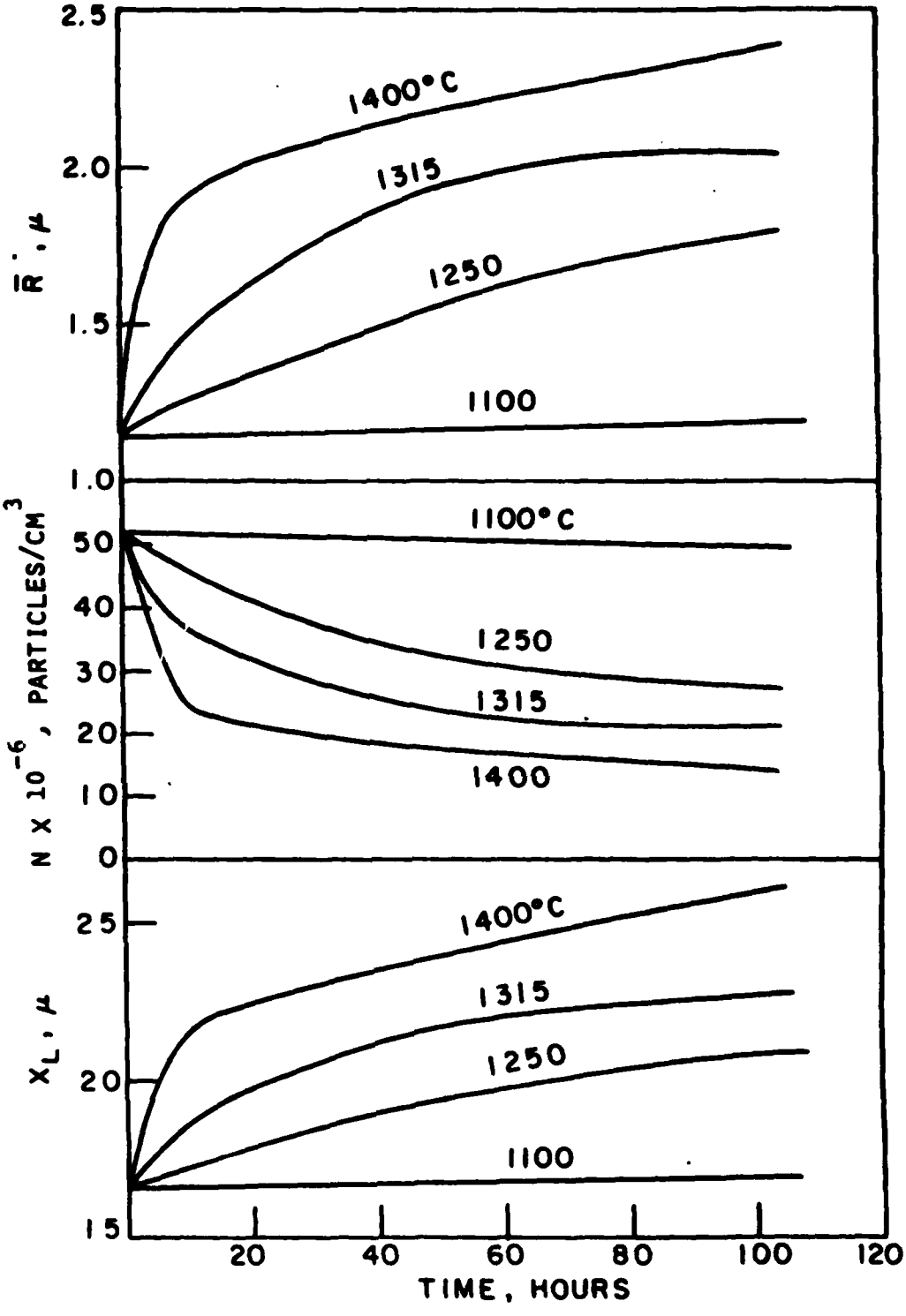

Figure 12 The effect of homogenization temperature on the coarsening of manganese sulfide inclusions in steel in terms of average radius, number of particles, and average interparticle spacing. Calculations are for steel containing 0.61% Mn and 0.017% S.

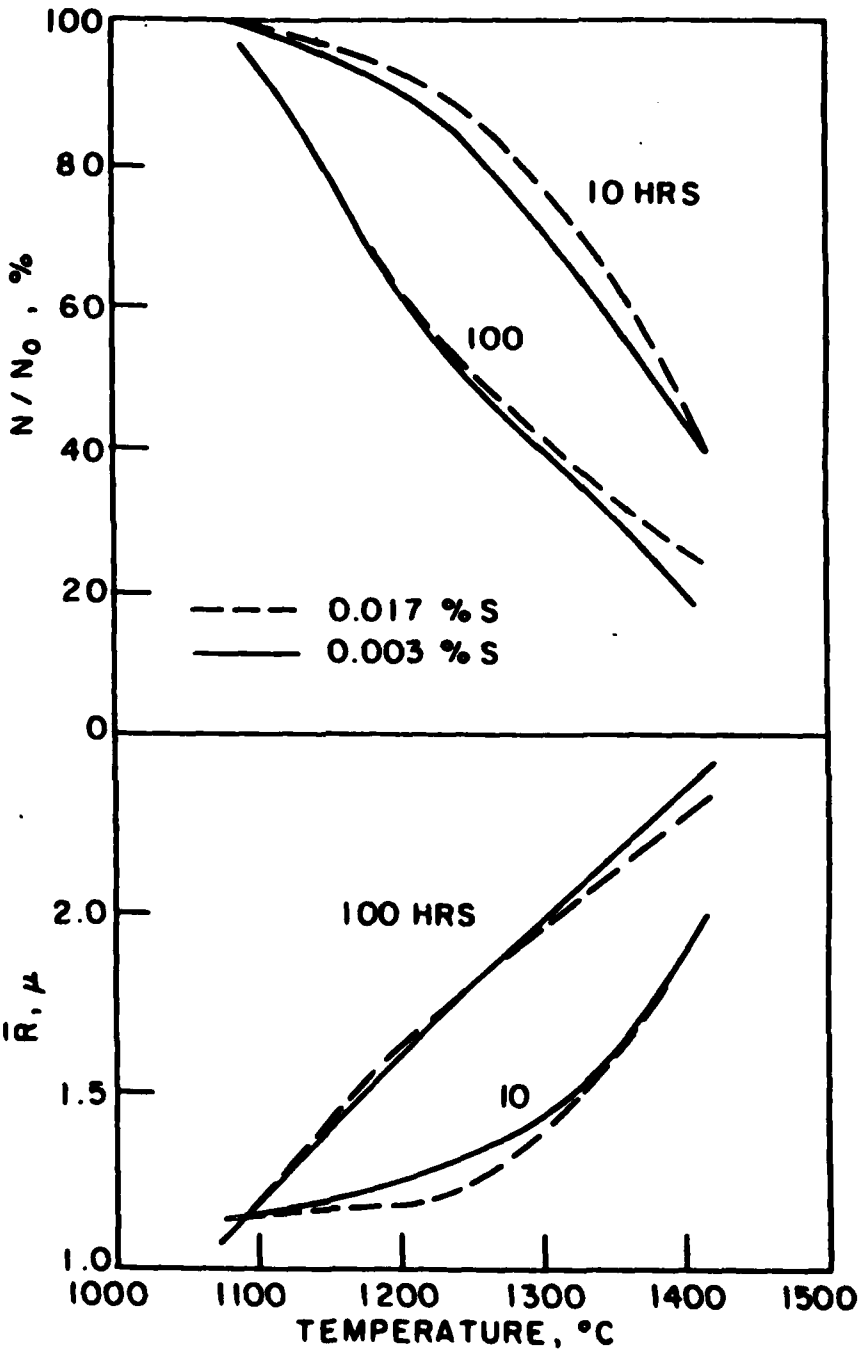

Figure 13 The relative number and average radius of undissolved sulfides in a steel containing 0.51% Mn calculated as a function of temperature.

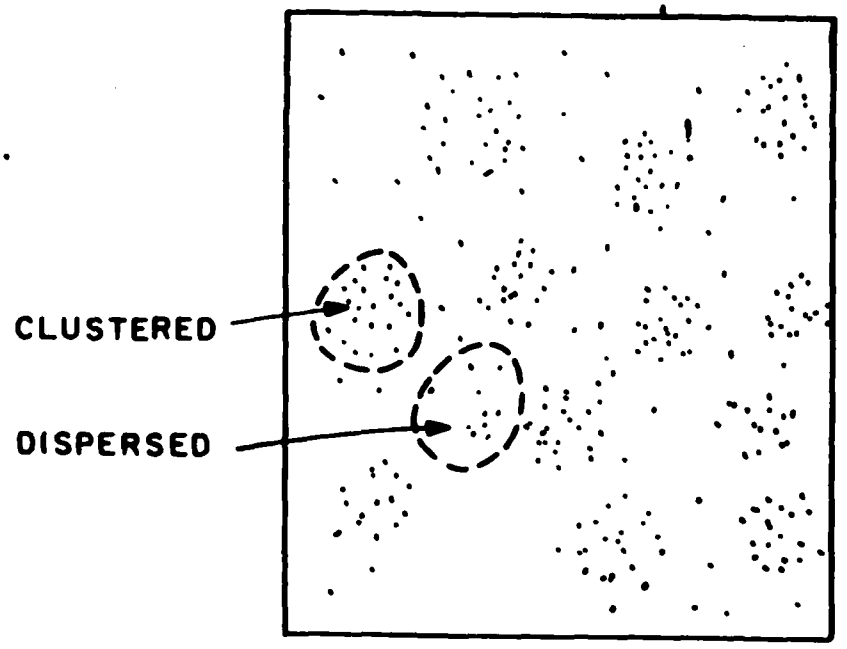

Figure 14 An example of a nonuniform distribution of particles showing clustered regions and dispersed regions.

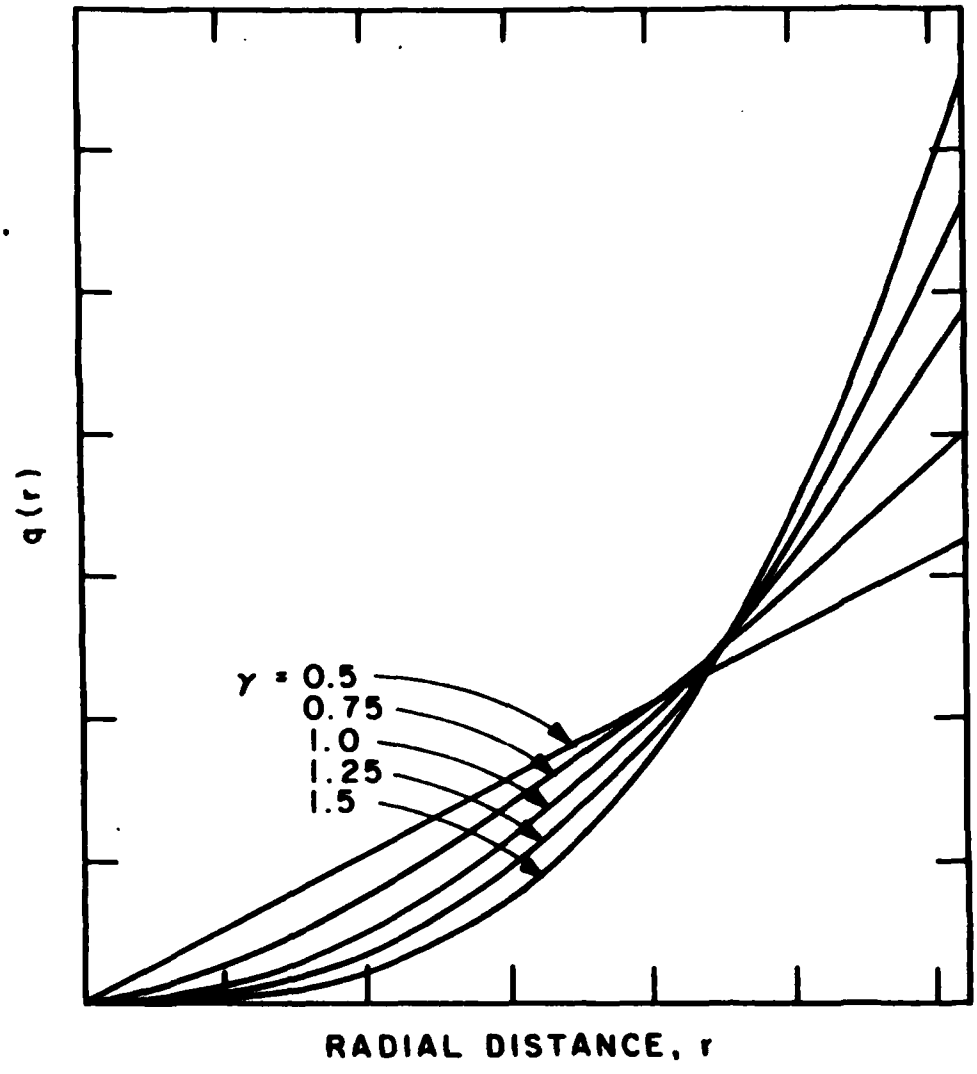

Figure 15 Space distribution function, q(r), for nonuniform particle distributions ($\alpha \neq 1$) and for a uniform distribution ($\alpha = 1$).

DISTRIBUTION LIST

No. of Copies	To
1	Office of the Under Secretary of Defense for Research and Engineering, The Pentagon, Washington, D. C. 20301
12	Commander, Defense Technical Information Center, Cameron Station, Building 5, 5010 Duke Street, Alexandria, Virginia 22314
1	Metals and Ceramics Information Center, Battelle Columbus Laboratories, 505 King Avenue, Columbus, Ohio 43201
	Deputy Chief of Staff, Research, Development, and Acquisition, Headquarters, Department of the Army, Washington, D. C. 20310
1	ATTN: DAMA-ARZ
	Commander, Army Research Office, P. O. Box 12211, Research Triangle Park, North Carolina 27709
1	ATTN: Information Processing Office
	Commander, U. S. Army Materiel Development and Readiness Command, 5001 Eisenhower Avenue, Alexandria, Virginia 22333
1	ATTN: DRCLDC
	Commander, U. S. Army Materiel Systems Analysis Activity, Aberdeen Proving Ground, Maryland 21005
1	ATTN: DRXSY-MP, H. Cohen
	Commander, U. S. Army Electronics Research and Development Command, Fort Monmouth, New Jersey 07703
1	ATTN: DELSD-L
1	DELSD-E
	Commander, U. S. Army Missile Command, Redstone Arsenal, Alabama 35809
1	ATTN: DRSMI-TB, Redstone Scientific Information Center
1	Technical Library
	Commander, U. S. Army Armament Research and Development Command, Dover, New Jersey 07801
2	ATTN: Technical Library
1	DRDAR-SCM, J. D. Corrie
1	DRDAR-SCM-P, Dr. J. Waldman
1	DRDAR-LCA, Mr. Harry E. Pebly, Jr., PLASTEC, Director
	Commander, U. S. Army Natick Research and Development Command, Natick, Massachusetts 01760
1	ATTN: Technical Library
	Commander, U. S. Army Satellite Communications Agency, Fort Monmouth, New Jersey 07703
1	ATTN: Technical Document Center

No. of Copies	To
	Commander, U. S. Army Tank-Automotive Research and Development Command, Warren, Michigan 48090
2	ATTN: DRDTA-UL, Technical Library
	Commander, White Sands Missile Range, New Mexico 88002
1	ATTN: STEWS-WS-VT
	Director, U. S. Army Ballistic Research Laboratory, Aberdeen Proving Ground, Maryland 21005
1	ATTN: DRDAR-TSB-S (STINFO)
	Commander, Dugway Proving Ground, Dugway, Utah 84022
1	ATTN: Technical Library, Technical Information Division
	Commander, Harry Diamond Laboratories, 2800 Powder Mill Road, Adelphi, Maryland 20783
1	ATTN: Technical Information Office
	Chief, Benet Weapons Laboratory, LCWSL, USA ARRADCOM, Watervliet, New York 12189
1	ATTN: DRDAR-LCB-TL
1	Dr. T. Davidson
1	Mr. D. P. Kendall
1	Mr. J. F. Throop
	Commander, U. S. Army Foreign Science and Technology Center, 220 7th Street, N. E., Charlottesville, Virginia 22901
1	ATTN: Military Tech, Mr. Marley
	Commander, U. S. Army Aeromedical Research Unit, P. O. Box 577, Fort Rucker, Alabama 36360
1	ATTN: Technical Library
	Director, Eustis Directorate, U. S. Army Air Mobility Research and Development Laboratory, Fort Eustis, Virginia 23604
1	ATTN: Mr. J. Robinson, DAVDL-E-MOS (AVRADCOM)
	U. S. Army Aviation Training Library, Fort Rucker, Alabama 36360
1	ATTN: Building 5906-5907
	Commander, U. S. Army Agency for Aviation Safety, Fort Rucker, Alabama 36362
1	ATTN: Library, Building 4905
	Commander, USACDC Air Defense Agency, Fort Bliss, Texas 79916
1	ATTN: Technical Library
	Commander, U. S. Army Engineer School, Fort Belvoir, Virginia 22060
1	ATTN: Library

No. of Copies	To
	Commander, U. S. Army Engineer Waterways Experiment Station, Vicksburg, Mississippi 39180
1	ATTN: Research Center Library
	Commander, U. S. Army Environmental Hygiene Agency, Edgewood Arsenal, Maryland 21010
1	ATTN: Chief, Library Branch
	Technical Director, Human Engineering Laboratories, Aberdeen Proving Ground, Maryland 21005
1	ATTN: Technical Reports Office
	Commandant, U. S. Army Quartermaster School, Fort Lee, Virginia 23801
1	ATTN: Quartermaster School Library
	Naval Research Laboratory, Washington, D. C. 20375
1	ATTN: Dr. J. M. Krafft - Code 5830
2	Dr. G. R. Yoder - Code 6384
	Chief of Naval Research, Arlington, Virginia 22217
1	ATTN: Code 471
	Air Force Materials Laboratory, Wright-Patterson Air Force Base, Ohio 45433
2	ATTN: AFML/MXE/E. Morrissey
1	AFML/LC
1	AFML/LLP/D. M. Forney, Jr.
1	AFML/MBC/Mr. Stanley Schulman
	National Aeronautics and Space Administration, Washington, D. C. 20546
1	ATTN: Mr. B. G. Achhammer
1	Mr. G. C. Deutsch - Code RW
	National Aeronautics and Space Administration, Marshall Space Flight Center, Huntsville, Alabama 35812
1	ATTN: R. J. Schwinghammer, EH01, Dir, M&P Lab
1	Mr. W. A. Wilson, EH41, Bldg. 4612
1	Ship Research Committee, Maritime Transportation Research Board, National Research Council, 2101 Constitution Ave., N. W., Washington, D. C. 20418
1	Librarian, Materials Sciences Corporation, Blue Bell Campus, Merion Towle House, Blue Bell, Pennsylvania 19422
	National Bureau of Standards, U. S. Department of Commerce, Washington, D. C. 20334
1	ATTN: Dr. R. Mehrabian
1	Mr. W. F. Anderson, Atomics International, Canoga Park, California 91303

No. of Copies	To
	United States Steel Corporation, Monroeville, Pennsylvania 15146
1	ATTN: Dr. G. R. Speich, Applied Research Laboratory
	Westinghouse Electric Company, Pittsburgh, Pennsylvania 15235
1	ATTN: Mr. R. E. Peterson, Research Laboratories
1	Mr. E. T. Wessel, Research and Development Center
	Hughes Helicopters, Centinella Avenue and Teala Street, Culver City, California 90230
1	ATTN: L. L. Soffa, M/S 305 T352
	Lukens Steel Company, Coatesville, Pennsylvania 19320
1	ATTN: Dr. Robert A. Swift
1	Mr. Joseph A. Ross, Jr.
	Materials Engineering Technology Laboratories, Irvine Industrial Complex, 1805 E. Carnegie Avenue, Santa Ana, California 92705
1	ATTN: Dr. L. Raymond
	Parker Hannifin Corporation, Bertea Control Systems Division, 18001 Von Karman Avenue, Irvine, California 92715
1	ATTN: C. Beneker
	Wyman-Gordon Company, Worcester, Massachusetts 01601
1	ATTN: Technical Library
	Lockheed-Georgia Company, 86 South Cobb Drive, Marietta, Georgia 30063
1	ATTN: Materials and Processes Engineering Dept. 71-11, Zone 54
	General Dynamics, Convair Aerospace Division, P.O. Box 748, Fort Worth, Texas 76101
1	ATTN: Mfg. Engineering Technical Library
1	Mechanical Properties Data Center, Belfour Stulen Inc., 13917 W. Bay Shore Drive, Traverse City, Michigan 49684
1	Dr. Robert S. Shane, Shane Associates, Inc., 7821 Carrleigh Parkway, Springfield, Virginia 22152
	Director, Army Materials and Mechanics Research Center, Watertown, Massachusetts 02172
2	ATTN: DRXMR-PL
1	DRXMR-PR
1	DRXMR-PD
1	DRXMR-AP
7	DRXMR-EM, Dr. G. Bruggeman

Army Materials and Mechanics Research Center Watertown, Massachusetts 02172 SULFIDE INCLUSIONS IN ELECTROSLAG REMELTED STEELS M. D. Boldy, T. Fujii, D. R. Poirier M. C. Flemings Massachusetts Institute of Technology Cambridge, KA 02139 Final Technical Report AMMRC-81-4, January 1981, 122 pp illus.-tables, Contract DAAG46-78-C-0032 D/A Project: 1L161102AH42: AMCMS Code, 61102A Final Report, December 1977 to December 1979	AD ____________ Unclassified Unlimited Distribution Key Words Precipitation Electroslag refining Alloy steels Overheating Inclusions Electron metallography Mathematical models Coarsening

The relationships among heat treatment, sulfide inclusion distribution and chemistry were investigated in this work, and the problem of overheating found to be directly related to these parameters. A basis for comparison was found in microscopic examination of carbon extraction replicas from commercially produced electroslag remelted steel. This showed a direct correlation between sulfide inclusion distribution and overheating. Further investigation characterized a critical cooling rate necessary for overheating to occur. Methods for eliminating the problem of sulfide inclusions in ESR steels were examined in detail. The simplest is to alter the cooling rate through the overheating range. Either a fast or a very slow cool eliminates the problem. An alternate method of eliminating the problem is to change the chemistry of the steel. These different techniques were examined in this work. All three were tested and proved to be successful in eliminating the sulfide problem. In an associated study a model to simulate the diffusion controlled coarsening and dissolution kinetics of particles. Within a metallic matrix was formulated. Calculations were made and compared with experiments in a model system and on manganese sulfide inclusions in iron. The effect of the manganese and sulfur content was studied. Agreement of the calculations is good.

Army Materials and Mechanics Research Center
Watertown, Massachusetts 02172
SULFIDE INCLUSIONS IN ELECTROSLAG REMELTED STEELS
M. D. Boldy, T. Fujii, D. R. Poirier
M. C. Flemings
Massachusetts Institute of Technology
Cambridge, MA 02139
Final Technical Report AMMRC-81-4, January 1981, 122 pp
illus.-tables, Contract DAAG46-78-C-0032
D/A Project: 1L161102AH42: AMCMS Code, 61102A
Final Report, December 1977 to December 1979
AD ____________
Unclassified
Unlimited Distribution
Key Words
Precipitation
Electroslag refining
Alloy steels
Overheating
Inclusions
Electron metallography
Mathematical models
Coarsening

The relationships among heat treatment, sulfide inclusion distribution and chemistry were investigated in this work, and the problem of overheating found to be directly related to these parameters. A basis for comparison was found in microscopic examination of carbon extraction replicas from commercially produced electroslag remelted steel. This showed a direct correlation between sulfide inclusion distribution and overheating. Further investigation characterized a critical cooling rate necessary for overheating to occur. Methods for eliminating the problem of sulfide inclusions in ESR steels were examined in detail. The simplest is to alter the cooling rate through the overheating range. Either a fast or a very slow cool eliminates the problem. An alternate method of eliminating the problem is to change the chemistry of the steel. These different techniques were examined in this work. All three were tested and proved to be successful in eliminating the sulfide problem. In an associated study a model to simulate the diffusion controlled coarsening and dissolution kinetics of particles. Within a metallic matrix was formulated. Calculations were made and compared with experiments in a model system and on manganese sulfide inclusions in iron. The effect of the manganese and sulfur content was studied. Agreement of the calculations is good.

Army Materials and Mechanics Research Center
Watertown, Massachusetts 02172
SULFIDE INCLUSIONS IN ELECTROSLAG REMELTED STEELS
M. D. Boldy, T. Fujii, D. R. Poirier
M. C. Flemings
Massachusetts Institute of Technology
Cambridge, MA 02139
Final Technical Report AMMRC-81-4, January 1981, 122 pp
illus.-tables, Contract DAAG46-78-C-0032
D/A Project: 1L161102AH42: AMCMS Code, 61102A
Final Report, December 1977 to December 1979
AD ____________
Unclassified
Unlimited Distribution
Key Words
Precipitation
Electroslag refining
Alloy steels
Overheating
Inclusions
Electron metallography
Mathematical models
Coarsening

The relationships among heat treatment, sulfide inclusion distribution and chemistry were investigated in this work, and the problem of overheating found to be directly related to these parameters. A basis for comparison was found in microscopic examination of carbon extraction replicas from commercially produced electroslag remelted steel. This showed a direct correlation between sulfide inclusion distribution and overheating. Further investigation characterized a critical cooling rate necessary for overheating to occur. Methods for eliminating the problem of sulfide inclusions in ESR steels were examined in detail. The simplest is to alter the cooling rate through the overheating range. Either a fast or a very slow cool eliminates the problem. An alternate method of eliminating the problem is to change the chemistry of the steel. These different techniques were examined in this work. All three were tested and proved to be successful in eliminating the sulfide problem. In an associated study a model to simulate the diffusion controlled coarsening and dissolution kinetics of particles. Within a metallic matrix was formulated. Calculations were made and compared with experiments in a model system and on manganese sulfide inclusions in iron. The effect of the manganese and sulfur content was studied. Agreement of the calculations is good.

Army Materials and Mechanics Research Center
Watertown, Massachusetts 02172
SULFIDE INCLUSIONS IN ELECTROSLAG REMELTED STEELS
M. D. Boldy, T. Fujii, D. R. Poirier
M. C. Flemings
Massachusetts Institute of Technology
Cambridge, MA 02139
Final Technical Report AMMRC-81-4, January 1981, 122 pp
illus.-tables, Contract DAAG46-78-C-0032
D/A Project: 1L161102AH42: AMCMS Code, 61102A
Final Report, December 1977 to December 1979
AD ____________
Unclassified
Unlimited Distribution
Key Words
Precipitation
Electroslag refining
Alloy steels
Overheating
Inclusions
Electron metallography
Mathematical models
Coarsening

The relationships among heat treatment, sulfide inclusion distribution and chemistry were investigated in this work, and the problem of overheating found to be directly related to these parameters. A basis for comparison was found in microscopic examination of carbon extraction replicas from commercially produced electroslag remelted steel. This showed a direct correlation between sulfide inclusion distribution and overheating. Further investigation characterized a critical cooling rate necessary for overheating to occur. Methods for eliminating the problem of sulfide inclusions in ESR steels were examined in detail. The simplest is to alter the cooling rate through the overheating range. Either a fast or a very slow cool eliminates the problem. An alternate method of eliminating the problem is to change the chemistry of the steel. These different techniques were examined in this work. All three were tested and proved to be successful in eliminating the sulfide problem. In an associated study a model to simulate the diffusion controlled coarsening and dissolution kinetics of particles. Within a metallic matrix was formulated. Calculations were made and compared with experiments in a model system and on manganese sulfide inclusions in iron. The effect of the manganese and sulfur content was studied. Agreement of the calculations is good.

UNCLASSIFIED
SECURITY CLASSIFICATION OF THIS PAGE (When Data Entered)

REPORT DOCUMENTATION PAGE	READ INSTRUCTIONS BEFORE COMPLETING FORM
1. REPORT NUMBER: AMMRC TR-81-4	2. GOVT ACCESSION NO.: AD A097469
3. RECIPIENT'S CATALOG NUMBER	
4. TITLE (and Subtitle): SULFIDE INCLUSIONS IN ELECTROSLAG REMELTED STEELS.	5. TYPE OF REPORT & PERIOD COVERED: Final Report. Dec 77 - Dec 79
	6. PERFORMING ORG. REPORT NUMBER
7. AUTHOR(s): M. D. Boldy, T. Fujii, D. R. Poirier and M. C. Flemings	8. CONTRACT OR GRANT NUMBER(s): DAAG46-78-C-0032 new
9. PERFORMING ORGANIZATION NAME AND ADDRESS: Massachusetts Institute of Technology, Cambridge, Massachusetts 02139	10. PROGRAM ELEMENT, PROJECT, TASK AREA & WORK UNIT NUMBERS: D/A Project 1L161102AH42, AMCMS Code: 61102A
11. CONTROLLING OFFICE NAME AND ADDRESS: Army Materials and Mechanics Research Center, ATTN: DRXMR-AP, Watertown, Massachusetts 02172	12. REPORT DATE: January 1981
	13. NUMBER OF PAGES: 122
14. MONITORING AGENCY NAME & ADDRESS (if different from Controlling Office)	15. SECURITY CLASS. (of this report): Unclassified
	15a. DECLASSIFICATION/DOWNGRADING SCHEDULE

16. DISTRIBUTION STATEMENT (of this Report)

Approved for public release; distribution unlimited.

17. DISTRIBUTION STATEMENT (of the abstract entered in Block 20, if different from Report)

18. SUPPLEMENTARY NOTES

19. KEY WORDS (Continue on reverse side if necessary and identify by block number)

Electroslag refining	Precipitation
Alloy steels	Coarsening
Overheating	Electron metallography
Inclusions	Mathematical models

20. ABSTRACT (Continue on reverse side if necessary and identify by block number)

The relationships among heat treatment, sulfide inclusion distribution and chemistry were investigated in this work, and the problem of overheating found to be directly related to these parameters.

A basis for comparison was found in microscopic examination of carbon extraction replicas from commercially produced electroslag remelted steel. → next page

(over)

DD FORM 1 JAN 73 1473 EDITION OF 1 NOV 65 IS OBSOLETE

409463

UNCLASSIFIED
SECURITY CLASSIFICATION OF THIS PAGE (When Data Entered)

Block No. 20

This showed a direct correlation between sulfide inclusion distribution and overheating. Further investigation characterized a critical cooling rate necessary for overheating to occur.

Methods for eliminating the problem of sulfide inclusions in ESR steels were examined in detail. The simplest is to alter the cooling rate through the overheating range. Either a fast or a very slow cool eliminates the problem. An alternate method of eliminating the problem is to change the chemistry of the steel. These different compositions were examined in this work. All three were tested and proved to be successful in eliminating the sulfide problem.

In an associated study a model to simulate the diffusion controlled coarsening and dissolution kinetics of particles within a metallic matrix was formulated. Calculations were made and compared with experiments in a model system and on manganese sulfide inclusions in iron. The effect of composition of manganese and of sulfur content was studied. Agreement of calculations is good.


LME